On the Possibility of Detecting Low Barrier Hydrogen Bonds with UV Spectroscopy and Kinetic Measurements

Jeff Miller

A Thesis Submitted to the
University of North Carolina at Wilmington in Partial Fulfillment
Of the Requirements for the Degree of
Master of Science

Department of Chemistry

University of North Carolina at Wilmington

2003

Approved by

Advisory Committee

_____ _____

_____
Chair

Accepted by

_____
Dean, Graduate School

TABLE OF CONTENTS

ABSTRACT

Recent Experimental evidence has pointed that in many enzyme-catalyzed biochemical pathways a short, strong hydrogen bond between an enzyme and substrate leads to an important contribution to enzyme catalysis. These bonds are termed low barrier hydrogen bonds. In this paper we show that the presence of low barrier hydrogen bonds can be determined in systems by UV spectroscopy and kinetic measurements.

In using the time-dependent view of UV spectroscopy, we apply several different UV spectra: photoabsorption, photodissociation, and emission, on systems containing a low barrier hydrogen bond. We find several distinguishing features in the UV spectra for systems that possess a low barrier hydrogen bond.

In using kinetic measurements, we find non-trivial differences among rate constant ratios of protonated to deuterated hydrogen bonds between strong and weak hydrogen bonds of proton transfer between donor and acceptor sites. This kinetic isotope effect is determined by performing full dynamic calculations of these rate constants by computing reactive flux through a dividing surface. This reactive flux is computed by evolving classical trajectories on an effective quantum mechanical potential energy surface.

ACKNOWLEDGEMENTS

I would like to thank Dr. Mike Messina for his time, knowledge and continued support. It's been a rewarding and unforgettable experience.

I would also like to acknowledge my family, whose love and support have been priceless along the way.

DEDICATION

I would like to dedicate this thesis to my parents, Harold and Carol Miller, whose outlook on life and personal appreciation for higher education have kept me constantly pushing forward.

LIST OF TABLES

LIST OF FIGURES

CHAPTER 1

INTRODUCTION

As the hydrogen atom becomes bonded to a highly electronegative atom (oxygen, fluorine, nitrogen) which in turn becomes strongly attracted to the lone electron charge of the hydrogen, a positive charge will exist on the other side of the hydrogen atom. This positive charge will become attracted to other unshared electrons on other electronegative atoms. Strong hydrogen bonds are formed when these atoms are strongly electronegative. This attraction can be intermolecular (long chains of molecules, i.e. proteins, enzymes) or intramolecular (bonding within the same molecule). Proteins consist of amino acids linked together by peptide bonds. The secondary or higher order structures of proteins are due to hydrogen bonding. The energy of a hydrogen bond is about 21 kJ/mol, about 5-10 percent of the energy of a normal single covalent bond.

Sometimes hydrogen bonds can stabilize transition states in enzyme catalyzed biochemical pathways. Thus increasing the rates of these reactions by several orders of magnitude. These hydrogen bonds are shorter and stronger than conventional hydrogen bonds. These short strong hydrogen bonds are termed low barrier hydrogen bonds (LBHB's). [1-10]

LBHB's are covalently bonded to a donor site and hydrogen bonded to the acceptor site. LBHB's will have low donor-acceptor distances (< 2.7 Å) and will have minimal barrier energies (< 20 kJ/mol) for the H atom to overcome during its donor to acceptor transition. This low donor-acceptor distance and minimal barrier energy enables the proton to move back and forth between the donor and acceptor sites. As the donor-acceptor distance drops to ~2.5 Å, the proton becomes essentially covalently bonded to

the donor and acceptor atoms. LBHB's seem to form when the pKa's of the acceptor and donor molecules are similar. Also, LBHB's are more favorably formed by the absence of a hydrogen bonding solvent such as water. The low donor-acceptor distances seem to keep the water pushed out of the LBHB environment. The lower the donor acceptor distance the stronger the LBHB.

An example of similar pKa's between donor and acceptor can be seen during the enzymic reaction catalyzed by a ketosteroid isomerase. A dienol or dienolate intermediate is formed from a reacting ketone. At the initial reaction Tyr^{14} is hydrogen bonded to the carbonyl oxygen of the ketone group. In this hydrogen bond the pKa of the Tyr^{14} is 11.6 and the pKa of the ketone group is negative. But when the dienol intermediate is formed the pKa raises to [10 in water, but higher on the enzyme], making the pKa's similar and the hydrogen bond becomes low barrier in character. Thus creating the energy to form the enol product. [1]

Another reaction that exhibits this type of matching pKa's is the mechanism of mandelate racemase. When a hydrogen is removed by 2 bases (Lys ^{166}, His ^{297}) an aci-carboxylate intermediate is formed. At the initial reaction Glu^{317} (pKa ~ 6.6) is hydrogen bonded to the carbonyl oxygen (pKa ~3.4). The formation of the aci-carboxylate intermediate raises the pKa of the enol oxygen up to 6.6, which makes a close match to the pKa of the Glu^{317}. Thus forming a LBHB which stabilizes the reaction. [1]

LBHB's can be detected through x-ray [9] and neutron diffraction, NMR [10] and IR [15] data. Another determining factor for the presence of LBHB's are the low values of the fractionation factor. Many people have found that low values of the isotopic

fractionation factor correlate with LBHB's. [7-8] This is the equilibrium constant for a reaction where H is replaced by D, deuteron. LBHB's can also be determined by low donor to acceptor distances (< 2.7 Å). Where regular Hydrogen bonds have lengths between 2.8 and 3.0 angstroms. Also, LBHB's have higher energy of formations (42-84 kJ/mol) than regular hydrogen bonds (~21 kJ/mol), which helps to drive reactions to completion.

Low Temperature x-ray and neutron diffraction studies were performed on benzoylacetone (1-phenyl-1,3-butadione) to study the presence of intramolecular hydrogen bonding. Benzoylacetone has a cis-enol system with a short intramolecular O-H- O hydrogen bond. The hydrogen bond seems to possess Low barrier qualities. The donor-acceptor distance is 2.502 Å, which fits the LBHB criteria of less than 2.7 Å. Also, the hydrogen bond is short compared to a normal ionic hydrogen bond. The two O-H distances were measured to be 1.329 Å and 1.245 Å. [11]

NMR can be a useful tool in determining LBHB's. As the LBHB strengthens, by the shortening of the distance between the donor and acceptor atoms from 3.0 Å to 2.4 Å, the proton becomes more deshielded causing its resonance to shift downfield. Strong LBHB's can reach downfield as far as 21 ppm. Where weak LBHB's shift downfield to 12 ppm.

An example of this can be seen with triosephosphate isomerase. An O-H-O low barrier hydrogen bond was found using NMR studies, which gave a chemical shift of 14.9 ppm corresponding to a donor-acceptor distance of 2.57 Å ± 0.05 Å. [12]

Another example of this downfield shift can be seen with the ketosteroid isomerase. Again a O-H-O low barrier hydrogen bond was found using NMR technology. The chemical shift of this low barrier hydrogen bond was found to be 18.2 ppm corresponding to a donor-acceptor distance of 2.49 Å ± 0.02 Å. [12]

As the LBHB becomes stronger and stronger the Infrared stretching frequencies become broader and are shifted to lower frequencies. [13] In an A-H--B hydrogen bond, as the hydrogen bond becomes a stronger and stronger LBHB the A-H distance (covalent bond) increases, the B-H distance decreases, and the A-B distance decreases, until the proton is placed symmetrically between the electronegative atoms of A and B, and it's bonding to A and B is basically covalent. This overall strengthening of the hydrogen bond will lower the IR stretching frequency.

A typical O-H-O hydrogen bond, with donor-acceptor distance of 3.0 Å, will have a stretching frequency of 3500 cm^{-1}. As the hydrogen bond develops low barrier characteristics the hydrogen stretching frequency will decrease. When the hydrogen bond becomes a strong LBHB, with a donor-acceptor distance of 2.3 Å, the new stretching frequency can be as low as 1500 cm^{-1}. These values will change slightly when the O atom is replaced by other electronegative atoms. But, with Infrared spectroscopy, there is always a downward shift to lower frequencies as the hydrogen bond becomes low barrier in character. [13]

A hydrogen bond between two heteroatoms can be well described by a double well potential energy function. The left well represents the configuration when the hydrogen atom is covalently bonded to the donor heteroatom. The right well represents the configuration when the hydrogen atom is covalently bonded to the acceptor

heteroatom. The barrier in between the two wells represents the amount of energy needed for the hydrogen atom to migrate between donor and acceptor heteroatoms. In a weak hydrogen bond the heteroatoms are greater than 2.7 Å apart and the energy barrier is high, greater than 20 kJ/mol. As the hydrogen bond forms low barrier characteristics, this energy barrier begins to decrease. Low barrier hydrogen bond energy barriers are usually less than 20 kJ/mol. The heteroatom distance is now about 2.5 to 2.6 Å. As the heteroatoms move closer together, the distance can decrease to as low as 2.45 to 2.3 Å, and the energy barrier disappears. Thus creating a single well potential energy function, where the hydrogen atom is equally bonded to both heteroatoms. An example of the no barrier hydrogen bond is the HF_2^{-1} molecule. The distance between the fluorine atoms was found to be 2.26 Å. Although these super strong hydrogen bonds are very rare

CHAPTER 2

USING UV SPECTRA IN DETERMINING LBHB's

This paper shows that UV spectra can be used as a tool to determine the presence of low-barrier hydrogen bonds in molecular structures. We look at several different types of simulated UV spectra on structures containing low-barrier hydrogen bonds. These different types of UV spectra are: photodissociation, absorption, and emission. The UV spectra is simulated using the time-dependent view of UV spectroscopy.

In the UV absorption simulation we assume that the UV photon takes the molecule of the ground electronic state to the excited electronic state in a harmonic fashion. Thus the proton will be either localized on the donor or acceptor atom in the excited electronic state. In the emission simulation we assume that the excited electronic state is harmonic and the molecule will emit down to the double-well potential of the ground state. In the photodissociation simulation we assume a repulsive excited electronic state. This is where the hydrogen atom is not bound to either the donor or acceptor atom. The UV photon will cause a break in the hydrogen – donor bond, while taking the molecule to the excited electronic state.

TIME DEPENDENT VIEW OF UV SPECTROSCOPY

All the simulations of the UV spectra are performed using time-dependent quantum mechanics. The time dependent view of spectral properties has gained wide acceptance in the last 25 years. [16] This view of spectroscopy relies on the solution of the time-dependent Schrodinger equation. The calculation of energies and Franck-Condon factors are replaced by the formation and Fourier transform of a time dependent correlation function. It is determined that the time dependent view of UV spectral properties on LBHBs show distinct and characteristic patterns.

The Fermi-golden rule equation for absorbance at laser frequency, $\omega_{L,}$ $\Sigma(\omega_L),$ is given by [17]

$$\sum(\omega_L) = \frac{\sum_{i_{gr}} e^{-BE_{i_{gr}}} \sum_{f_{ex}} \left|\left\langle i_{gr} \mid f_{ex} \right\rangle\right|^2 \delta\left[\omega_L - \left(E_{f_{ex}} - E_{i_{gr}}\right)\right]}{\sum_{i_{gr}} e^{-BE_{i_{gr}}}} \tag{1}$$

The i_{gr} is the index that represents the i^{th} vibrational eigenstate within the ground electronic state, with the energy $E_{i_{gr}}$. The index f_{ex} represents the f^{th} vibrational eigenstate found on the excited electronic state, with energy $E_{f_{ex}}$. The spectrum must be Boltzmann averaged over the initial states i_{gr} at inverse temperature β or (1/ kT). The term $\left|\left\langle i_{gr} \mid f_{ex} \right\rangle\right|^2$ is the Frank-Condon factor which gives the height of each absorption line in the spectrum. The Frank-Condon factor is the probability of making the transition

from the initial state to the final state and is the overlap of the initial and final wavefunctions.

$$\mathrm{Pr}\,ob - i \to f \propto \left| \int dx \Psi_i(x) \Psi_f(x) \right|^2 = \left| \left\langle i_{gr} \,\middle|\, f_{ex} \right\rangle \right|^2 \tag{2}$$

The $\delta\left[\omega_L - \left(E_{f_{ex}} - E_{i_{gr}}\right)\right]$ term is the Dirac δ-function that places each absorption line at it's proper corresponding energy in the UV spectrum. When a molecule absorbs a photon, energy must be conserved. That is, the photon energy, ω_L, for each absorption is exactly equal to the energy difference of initial and final states, $\omega_L = E_{f_{ex}} - E_{i_{gr}}$. This is the Bohr frequency rule and it must be satisfied for proper positioning of each absorbance line.

The well-known conversion of the time-independent Fermi-golden rule into the time-dependent Fermi-golden rule is given by [14]

$$\sum\left(\omega_L\right) = \frac{\sum_{i_{gr}} e^{-BE_{i_{gr}}} \left(\frac{\mathrm{Re}}{\pi}\right) \int_0^t dt e^{-i\left(\omega_L - E_{i_{gr}} + i\Gamma\right)t} C_{i_{gr}}(t)}{\sum_{i_{gr}} e^{-BE_{i_{gr}}}} \tag{3}$$

Where $C_{i_{gr}}(t)$ is the auto-correlation function of the initial state (i_{gr}) wave function

$$C_{i_{gr}}(t) = \left\langle i_{gr} \left| e^{-iH_{ex}t} \right| i_{gr} \right\rangle \tag{4}$$

The correlation function is obtained by propagating each initial wavefunction to its corresponding wavefunction in the excited state and measuring the overlap with respect to time. The initial ground state wavefuntion is propagated to the excited state by $e^{-iH_{ex}t}$. The damping factor in Eq. (3), Γ, gives the absorbance line width and is important in obtaining viable results when one Fourier transforms the Correlation function. The absorbance spectra is obtained by performing the Fourier transform on the correlation function at laser frequency, ω_L. The correlation function is computed by propagating in time the initial state wavefunction, $\langle i_{gr} |$,by solving the time-dependent Schrodinger equation (TDSE)

$$\hat{H}_{ex}\phi_{i_{gr}}(x,t) = i\eta\frac{\partial\phi_{i_{gr}}}{\partial t}(x,t) \tag{5}$$

Where $\hat{H}_{ex}$ is the Hamiltonian operator for the excited electronic state

$$\hat{H}_{ex} = \hat{T} + \hat{V}_{ex}(x)\,. \tag{6}$$

Where $\phi_{i_{gr}}(x,t)$ is the time-dependent wave function, $\hat{V}_{ex}(x)$ is the potential energy operator and $\hat{T}$ is the kinetic energy operator.

POTENTIAL ENERGY SURFACES FOR PHOTODISSOCIATION, ABSORPTION, AND EMISSION

We now explain the potential energy surfaces used to simulate UV spectra in photodissociation, absorption, and emission.

(1) The Ground Electronic State

It is assumed that the ground electronic state will contain the LBHB. It seems valid to assume that these short, strong, and stable hydrogen bonds will be found in their molecular systems ground electronic state. It has been shown in recent publications that a quadratic-quartic is capable of describing a proton coordinate in a LBHB system [19]. Therefore, the potential energy surface representing the ground electronic state is:

$$V(x) = Ax^4 - Bx^2 + D \tag{7}$$

Where A and B are coefficients that determine the barrier height D and the curvature of the well, k. Here D and k are:

$$D = \frac{B^2}{4A} \tag{8a}$$

$$k = 4B \tag{8b}$$

This potential energy surface for the ground state is shown in figure 1(a). Table 1 shows different sets of A and B coefficients, which give different barrier heights/LBHB strengths.

(2) Excited Electronic State: Photodissociation

In Photodissociation it is assumed that the hydrogen bond is cleaved when it is propagated up to the excited electronic state by the UV photon. Therefore, the hydrogen atom isn't bound to either electronegative atom and the excited electronic state is completely repulsive. Photodissociation can also be obtained if the system is propagated to the high side on the hard, repulsive wall of the harmonic electronic excited state. The potential energy surface for a purely repulsive state will be represented by:

$$V(x) = Ce^{-\delta x} \tag{9}$$

Here C and δ are constants. Where C sets the energy of the surface (relative to the ground state minimum) and δ sets the steepness of the potential. This potential function is shown in Fig. 1 (a).

(3) Excited Electronic States: Absorption and Emission

The excited electronic state will be assumed to be harmonic in both absorption and emission. Secondly, we will assume that the proton will be localized on either the donor or acceptor atom in the electronic excited state. This means there will be a strengthening of the covalent bond and a weakening of the hydrogen bond. Thus, the minimum of the excited electronic state should be directly above one of the well minima of the ground electronic state. The potential energy surface for the harmonic excited state of absorption and emission will be:

$$V(x) = \frac{\mu\omega^2}{2}(x-\gamma)^2 \tag{10a}$$

$$\gamma = \sqrt{\frac{B}{2A}} \tag{10b}$$

Where γ is the parameter that shifts the minimum of the electronic excited state directly above one of the minimum of the double-well potential of the ground electronic state. This potential energy surface is shown in Figure 1(b).

RESULTS AND DISCUSSION

For all simulations of UV absorption, the ground electronic state is taken as the double-well potential given in Eq. (7). By varying the A and B parameters we can obtain a range of barrier heights in the double-well potential. This range of barrier heights include high barrier heights (weak hydrogen bonds) to low barrier heights (strong hydrogen bonds). The three double-well potentials we will study are in Table 1. For each double well potential we compute the eigenstates by solving the TDSE for the double-well potential in Eq. (7). The wavefunction is expanded in a basis set of particle in a box eigenfunctions. It is found that a box length of L = 4 Å and 50 particle in a box basis functions is adequate for the results to converge.

For the double-well potentials in table 1 the two lowest eigenstates are responsible for greater than 99% of the value of the partition function. Thus only the two lowest eigenstates needed to be propagated in order to compute the Boltzmann averaged spectra given by Eq. (3).

Figures 2(a) and 2(b) show the lowest eigenstates of the double-well potential that have barrier heights of 65.6 kJ mol^{-1} and 8.0 kJ mol^{-1}, respectively. It can be seen that as the barrier height decreases the distance between the two maxima of the wavefunction decreases.

This trend can be explained by equations 8(a) and 10(b). As the barrier height D decreases, B decreases and A increases. This leads to smaller values of γ. Since γ places the maxima of the wavefunction over the minima of the double-well potential, then the separation between maxima of the wavefunction will decrease upon decreasing barrier height.

The initial ground states (lowest and 1st excited vibrational states) are propagated to the electronic excited state by solving the TDSE in Eq. (5). The TDSE is solved by using the Feit-Fleck split operator technique [20]. The wavefunction is discretized on a spatial grid of 1024 points with a length of 5 Å. The time step in propagation is 1 x 10^{-1} fs for all simulations. The correlation function is formed by overlapping the propagated wavefunction with itself as the wavefunction evolves in time on the electronic excited state. The absorption spectra is then determined by a Fourier transform of this correlation function (see Eq. 3). We multiply all correlation functions by an exponentially decaying factor that damps the correlation to less than 1 x 10^{-4} by a time of 100 fs. This gives all absorption and emission lines in the spectra a Lorentzian line width of ~ 50 cm^{-1}.

(A) Absorption

(1) Photodissociation Spectra

Figures 3(a), (b), and (c) show the photodissociation spectra for systems with double-well potentials having barrier heights of 65 kJ mol^{-1}, 16 kJ mol^{-1}, and 8 kJ mol^{-1}, respectively. The potential energy parameters of the excited repulsive state in Eq. (9) are C = 8790 cm-1 and δ = 5 x 10^{9} m^{-1}. Each photodissociation spectral graph shows 2 distinct absorbances in the UV spectra. These two distinct absorbances result from the time dependent view of spectroscopy and can be explained. Figure 4 shows the correlation functions of the LBHB's with barrier heights of 65 kJ mol^{-1} and 8 kJ mol^{-1} that give rise to the photodissociation spectra in Fig's 3(a) and 3(c). It can be seen that each correlation function has a recurrence between 5 and 10 fs. The Fourier transform of a time series containing a single recurrence will show two absorption peaks at two distinct frequencies. This recurrence is due to the overlap of the initial wavefunction and the time

evolving wavefunction on the excited state. Figure 5 shows the initial wavefunction (solid line) on the ground electronic state at a time of zero for a barrier height of 8 kJ mol $^{-1}$. It also shows the time evolving wavepacket (dashed line) on the excited electronic state at a time of 10 fs for a barrier height of 8 kJ mol $^{-1}$. It can be seen that the wavepacket on the electronic excited state overlaps the right maximum of the initial wavefunction causing the recurrence. In figure 4, the correlation function for a double-well potential with a barrier height of 8 kJ mol $^{-1}$ is shown as the dashed line. The recurrence occurs at 7.5 fs. Therefore, the distance between the two spectral peaks should be 2π / 7.5 fs. This corresponds to about 4500 cm^{-1} which matches the distance between spectral peaks in Fig. 3(c). If no LBHB were present and the ground state was completely harmonic with a vibrational frequency of 2300 cm^{-1} then the spectra in Fig. (6) would occur. The spectra that arises from the excitation of a harmonic ground state to a repulsive excited state contains a single spectral peak. Therefore, a system containing a photodissociative excited state with a LBHB will have 2 distinctive absorption peaks, while a system containing a photodissociative excited state without a LBHB will have only a single absorption peak. Also, as the strength of the LBHB increases the distance and resolution of the two peaks decrease. We have performed many simulations using different sets of photodissociation constants C and δ, and have obtained similar results as described above.

(2) Photoabsorption Spectra

The photoabsorption spectra that arises from the excitation of a double-well ground state to a harmonic excited state can be seen in Figs. 7(a) and 7 (b). Fig. 7(b) shows the spectra that arise when the double-well ground state has a LBHB (barrier of 8 kJ mol^{-1}). Fig. 7(a) shows the spectra that arises when the double well ground state has a weak

hydrogen bond (barrier of 65 kJ mol^{-1}). The functional form of this harmonic excited state is given in Eqs. (10). The excited state frequency is ω_e = 3000 cm^{-1} . This is a typical O-H vibrational frequency in an excited electronic state [21]. The strong LBHB, Fig. 7 (b), shows a large absorption peak at 1500 cm^{-1} followed by a Frank-Condon progression of vibronic lines. Each vibronic line is separated by 3000 cm^{-1} which is equal to the excited state frequency. The weak hydrogen bond, Fig. 7(a), shows no Frank-Condon progression. This progression is not absent, but shifted up to greater than 30,000 cm^{-1}. This large difference between the photoabsorption spectra of a system with a LBHB and a system without a LBHB can be explained by time-dependent spectroscopy.

The initial wavefunction of the double-well ground state has one maxima at the minimum of the electronic excited state of a photoabsorption system. While the other maxima is away from the minima, farther up in energy when excited. As this initial wavefunction is propagated up to the excited state, two components to the correlation function arise. One component occurs from the lobe maxima that is located at the excited state minima. When this lobe maxima is propagated up to the excited state minima, it becomes nearly stationary in time. This leads to a large absorption peak at the lower frequency side of the spectrum. The second component comes from the second lobe maxima which is away from the minima of the excited state. When this lobe maxima is propagated to the excited state it occurs high up on the energy wall of the harmonic excited state. This component of the wavepacket is far from equilibrium and will evolve back and forth harmonically over time. This component of the correlation function evolves in time with a frequency of the excited state vibration. When this component of

the correlation function is Fourier transformed it leads to the Frank-Condon progression in the photoabsorption spectra.

It has already been determined that as the LBHB grows stronger then the lobe maxima of the initial wavefunction become closer together and less resolved, Figs. 2(a) and 2(b). So, when the initial wavefunction of a system containing a LBHB is propagated up to the excited state, the lobe maxima that is away from the excited state minima isn't at a very large energy above the minima. Thus, the Frank-Condon progression in the photoabsorption spectrum for a system with a LBHB is not shifted that high up in energy. While for weak, high barrier hydrogen bonds the lobe maxima away from the minima is propagated to a high energy above the minima and the Frank-Condon progression in the photoabsorption spectra is severly blue-shifted. By comparison, Fig. (8) shows the photoabsorption spectra for a system with no LBHB that is propagated up to the harmonic excited state. There is no Frank-Condon progression when there is no LBHB. Therefore, the difference in photoabsorption spectra in a system with a LBHB and a system without a LBHB is a Frank-Condon vibronic progression that isn't blue-shifted.

(3) Emission

In Emisson, a harmonic electronic excited state emits down to a double-well ground state. The O-H vibrational frequency on the excited state is ω_e = 3000 cm^{-1}. Figs. 9(a) and 9(b) show the difference in emission spectra that result when one system has a weak, high barrier hydrogen bond (HBHB) verse one that has a strong, low barrier hydrogen bond. Fig. 9(a) is the emission spectra for a system with a barrier of 65 kJ/mol (HBHB) and Fig. 9(b) is the emission spectra for a system with a barrier of 8 kJ/mol (LBHB). Fig. 9(a) shows one large absorption peak at low cm^{-1}. In contrast, Fig.

9(b) shows a distinguishing feature in that the first emission maximum is split in two peaks. This double peak spectrum can be explained by the time dependent view of spectroscopy. The lowest eigenstate in the double-well ground state is at 10 kJ/mol. The LBHB barrier is at 8 kJ/mol. So, when the LBHB wavepacket is emitted down to the double-well potential it is above the barrier and cycles back and forth between the steep energy barriers of the double-well potential. The classical period for this motion is 60 fs. Thus, the distance between the emission peaks should be 500 cm^{-1}, which is shown in Fig. 9(b). The HBHB has a barrier height of 65 kJ/mol. When the HBHB wavepacket is emitted down to the lowest eigenstate of the double-well potential (10 kJ/mol) it becomes trapped in the well and is virtually stationary. This leads to the single absorbance maximum seen in Fig. 9(a). Therefore, an easily observed characteristic which can distinguish between LBHB and weak hydrogen bonds in the emission spectra is a secondary emission maximum.

CHAPTER 3

USING KINETIC MEASUREMENTS IN DETERMINING LBHB's

In the first part of this paper we have discussed several experimental methods used to determine the presence of LBHB's. These methods are mostly thermodynamic in design and measure a systems equilibrium properties.[5] In the second part of this paper we will show that another method which can be used to detect the presence of LBHB's in molecular systems is the kinetic measurement from the transfer of protons and deutrons between donor and acceptor sites in a molecule containing a hydrogen bond.

As stated earlier, fractionation factors are useful measurements in determining the presence of LBHB's. Since the fractionation factor is the equilibrium constant for a reaction in which the proton in a LBHB is replaced by a deuteron [7], it should not be unreasonable to assume variations of these rate constants will give insight into the determination of LBHB's as well.

The goal of this work is to quantify as rigourously as possible what kinetic isotope effects to expect in a proton transfer between donor and acceptor sites in a hydrogen bond. Also, to see how this kinetic isotope effect changes with hydrogen bond strength. This goal is achieved by computing rate constants for systems containing differing hydrogen bond strengths using trajectories to compute the reactive flux through a dividing surface.

Quantum Mechanical effects must be included in these calculations since the critical reaction coordinate involves the low-mass proton and deuteron. These quantum effects are included by propagating these trajectories onto an effective quantum mechanical potential energy surface. In a previous work, we have shown that such an

approach compares very well to the analogous exact quantum mechanical calculations based on the flux correlation function. [22]

It is known that a rate constant for proton transfer in an isolated double-well potentials do not exist. This is because systems that are below the barrier will never get enough energy to overcome it and systems that are above the barrier will constantly move back and forth between reactants and products. The only way for a system to successfully transfer a proton or deuteron across the barrier is for the system to be coupled with an outside source that can absorb or emit energy.

For this system we use a set of harmonic oscillators, that are coupled to the LBHB proton coordinate, to absorb or emit energy. The frequencies and couplings of these harmonic oscillators are chosen from a mapping of the Generalized Langeuin Equation [23] (GLE) to a system coordinate coupled to a discrete set of oscillators. Then a ratio of rate constants for deuteron to proton transfer is determined for several varying hydrogen bonded systems. These systems will vary between strong hydrogen bond strengths (LBHB) to weak hydrogen bond strengths (HBHB).

These hydrogen bonded systems will be coupled to several different sets of harmonic oscillators. These harmonic oscillator sets will contain a range of friction strengths and time scales that will help mimic varying solvent responses.

REACTIVE FLUX ON AN EFFECTIVE QUANTUM MECHANICAL POTENTIAL ENERGY SURFACE

The Classical formulation of the rate theory defines the rate constant as a reactive flux through a dividing surface separating reactants and products. This classical formulation predicts the rate constant, κ, is proportional to the plateau value of the reactive flux correlation function $C(\tau)$.[24]

$$C(\tau) = Q_R \kappa \tag{11}$$

Here Q_R is the reactant partition function and τ is an adequate amount of time for the correlation function to reach the plateau value. The classical expression for this correlation function is:

$$C(t) = \int d\vec{x}_0 d\vec{p}_0 e^{-\beta H(\vec{x}_0, \vec{p}_0)} \delta[Z] \dot{Z} \chi(\vec{x}(t), \vec{p}(t); \vec{x}_0, \vec{p}_0) \tag{12}$$

The set $(\vec{x}_0, \vec{p}_0)$ is the initial set of positions and momentums, Z is the functional form of the dividing surface separating products and reactants, and $\dot{Z}$ is the time derivative of Z. This time derivative is defined by the Poisson bracket of Z and the system Hamiltonian, H(x,p).

$$\dot{Z} = \{H, Z\} \tag{13}$$

This time derivative starts the trajectories on the dividing surface. The characteristic function $\chi(\vec{x}(t), \vec{p}(t); \vec{x}_0, \vec{p}_0)$ is the dynamic component of the correlation function and keeps track of which trajectories are on the product and reactant sides of the dividing surface at time, t. β is the inverse of the temperature, $\beta = 1/kT$, where k is the Boltzmann constant. The potential energy of our system is given by

$$V(x, \vec{y}) = V_{LBHB}(x) + \frac{m}{2}\sum_{j}^{N} \omega_j^2 (y_j - c_j x)^2 \tag{14a}$$

$$V_{LBHB}(x) = Ax^4 - Bx^2 + D \tag{14b}$$

Here V_{LBHB} is the double-well potential along the proton coordinate, x, of the LBHB.[19] The height of the barrier is given by D and it's related to A and B by D = $B^2/4A$. Our system uses a symmetric double well energy potential. It is known that one cannot experimentally tell the difference between the donor and acceptor sites in a symmetric double well energy potential. Thus, an experimental value for the rate constant for transfer between the donor and acceptor sites cannot be measured in a symmetric system. The symmetric double well potential is used because it is simpler and the goal of this work is to quantify what order of magnitude isotope effects are possible to be observed in varying strengths of hydrogen bonded systems. It was determined that slight asymmetries in the potential do not appreciably change the results.

The coordinates $\{\vec{y}\}$ represent the set of harmonic oscillators that couple to the LBHB coordinate. The frequencies, ω_j, and coupling, c_j, of these N oscillators are chosen from the well known mapping of the GLE.[23,25]

In a previous work one of us has shown that an effective quantum mechanical potential can be defined as [26]

$$V(x,\overline{\overline{y}}) = V_{Classical}(x,\overline{\overline{y}}) - \frac{1}{\beta}\ln\{W(x)\} \tag{15}$$

Here $W(x)$ is a weight function given by

$$W(x) = \prod_{j}^{N+1} \frac{\eta\beta\sqrt{\lambda_j(x)}}{2\sinh\left(\frac{\eta\beta\sqrt{\lambda_j(x)}}{2}\right)} \tag{16}$$

The $\{\lambda_j(x)\}$ are the eigenvalues of the force constant matrix whose elements are,

$$\left[\underset{\approx}{V}\right]_{11} = \frac{\partial^2 V}{\partial x^2} = 12Ax^2 - 2B + \sum_j \omega_j^2 c_j^2 \tag{17a}$$

$$\left[\underset{\approx}{V}\right]_{1j} = \frac{\partial^2 V}{\partial x \partial y_j} = -\omega_j^2 c_j \tag{17b}$$

$$\left[\underset{\approx}{V}\right]_{kk} = \frac{\partial^2 V}{\partial y_k \partial y_k} = \omega_k^2 \tag{17c}$$

If an eigenvalue is less than zero we treat the system coordinate, x, as a truncated parabolic barrier at point x.[27] Then the weight function takes a different form than in Eq. (16) and this is discussed in Refs. (26-27).

Since the eigenvalues of the force constant matrix are independent of the harmonic oscillator coordinates, $\vec{y}$, the weight function is only dependent on the hydrogen bond coordinate , x. This independence of the weight function is very convenient. When one wants to propagate classical trajectories on a potential energy surface one needs to calculate the derivative of the potential surface for each degree of freedom at each time step. This becomes very difficult and time consuming when the effective quantum potential is dependent on $\vec{y}$, since there is no simple analytical expression for the first derivative of the effective quantum potential. In our case, the solvent(bath) portion of the effective quantum potential is identical to the classical potential. Which makes the spatial first derivatives along these degrees of freedom easy to compute. It becomes very efficient to fit the $V_{LBHB}(x)$ portion of the classical potential to a quantumly effective quadratic-quartic potential containing new effective coefficients of A,B and D.

$$V_{LBHB}^{eff}(x) = A_{eff}\,x^4 - B_{eff}\,x^2 + D_{eff} \tag{18}$$

The new effective coefficients of A_{eff} and B_{eff} are needed to reproduce the effective quantum potential surface along the hydrogen bond axis, x. The new barrier height, D_{eff}, is determined by $D_{eff} = \frac{B_{eff}^2}{4A_{eff}}$. It will be seen that the new effective quantum potential has a lower barrier height than the classical potential surface. This is due to the tunneling and zero-point energy corrections.

The classical reactive flux correlation function (Eq. 12) is independent of the form

and placement of the dividing surface. This not being true when one propogates classical trajectories onto an effective quantum potential surface. Our dividing surface was chosen to be located at x = 0. With this positioning of the dividing surface and substituting the effective quantum potential for the classical potential the correlation coefficient in Eq. 12 can be written as

$$C(t) = e^{-\beta D_{eff}} \int dp_{x_0} d\varpi_0 d\varpi_{p_{y_0}} \frac{p_{x_0}}{\mu} e^{-\beta H_{eff}(x_0=0, p_{x_0}, \varpi_{y_0}, \varpi_{p_{y_0}})} \chi_{eff}(t) \qquad (19)$$

Here $\chi_{eff}(t)$ is the characteristic function as computed by running classical trajectories on the effective quantum potential energy surface.

The reactant partition function is obtained by evaluating matrix element V_{11} (Eq. 17a) at the well minima so V_{11} becomes $4B + \sum_j \omega_j^2 c_j^2$. The force constant matrix is diagonalized yielding a set of eigenvalues $\{\lambda_j\}$. The reactant partition function is then given by

$$Q_R = \prod_{j=1}^{N+1} \frac{1}{2\sinh\left\{\eta\beta \frac{\sqrt{\lambda_j}}{2}\right\}} \qquad (20)$$

The ratio of deuterated to protonated rate constants can now be written as

$$\frac{\kappa_D}{\kappa_H} = \left(\frac{Q_R^H}{Q_R^D} \right) e^{-\beta\left(D_{eff}^D - D_{eff}^H\right)} \frac{\left\langle \chi_{eff} \right\rangle_D}{\left\langle \chi_{eff} \right\rangle_H} \tag{21}$$

Here $\left\langle \chi_{eff} \right\rangle$ denotes the value of the integral in Eq. 19 at the plateau time, τ. The ratio of partition functions for protonated to deuterated species, i.e., $\left(\frac{Q_R^H}{Q_R^D} \right)$ in Eq. (21), is equal to the inverse of the isotopic fractionation factor, ϕ, giving

$$\frac{\kappa_D}{\kappa_H} = \left[\frac{e^{-\beta\left(D_{eff}^D - D_{eff}^H\right)}}{\phi} \right] \frac{\left\langle \chi_{eff} \right\rangle_D}{\left\langle \chi_{eff} \right\rangle_H} \tag{22}$$

With the first term in Eq. (22) possessing all the thermodynamic information of the rate constant ratio and the second term possessing the dynamical component.

RESULTS AND DISCUSSION

The rate constant ratios in Eq. (22) are calculated in two steps. The first step requires the calculation of all the thermodynamic information in Eq. (22). The effective quantum potentials are computed via Eqs. (15-17c) for differing bath friction strengths, friction time scales, and two LBHB potential energies, $V_{LBHB}(x)$. We consider a LBHB with A and B parameters of 0.07 a.u. and 0.04 a.u., respectively. This set of A and B parameters leads to a barrier height of 15 kJ/mol and thus represents a low barrier hydrogen bond. The other hydrogen bond has A and B parameters of 0.07 a.u. and 0.1 a.u., respectively. This leads to a large barrier of 94 kJ/mol, which is considered a weak hydrogen bond or a high barrier hydrogen bond.

A fast and slow friction time scale will be used to model the solvent movement. The slow friction time scale has σ = 800 fs, [for details see Eqs. (6-10) of Ref. (16)]. The rate constants exhibit the classical Kramer's turnover behavior with respect to friction strength. Where weak friction strength values will be before the turnover region and strong friction strength values will come after the turnover region.

The effective quantum potentials are computed for each friction strength and friction time scale using Eq. (15), and then fit the effective quantum potentials, $V_{LBHB}(x)$, to a quadratic-quartic functional form using new values of A and B (A_{eff}, B_{eff}) in Eq. (18).

The partition functions are calculated by evaluating the matrix element, V_{11}, at the will minima. Then the isotopic fractionation factor could be determined as the ratio of the deuterated to protonated partition functions.

The second part of the calculation of the ratio of the deuterated to protonated rate constants involves the computation of $\left\langle X_{eff} \right\rangle$, the dynamical component of the equation. To compute the dynamical component we must compute the plateau value of

$$\left\langle X_{eff} \right\rangle = \int dp_{x_0} d\varpi_{y_0} d\varpi_{p_{y_0}} \frac{p_{x_0}}{\mu} e^{-\beta H_{eff}(x_0=0, p_{x_0}, \varpi_{y_0}, \varpi_{p_{y_0}})} X_{eff}(t) \tag{23}$$

This is achieved by running classical trajectories on the effective quantum potential. The equations of motion for the special coordinates of the system and bath are,

$$\dot{p}_x = \frac{-\partial V_{eff}}{\partial x} = -4A_{eff}x^3 + 2Bx^2 + m\sum_{j=1}^{N} c_j \omega_j^2 (y_j - c_j x) \tag{24a}$$

$$\dot{p}_{y_j} = \frac{-\partial V_{eff}}{\partial y_j} = -m\omega_j^2 (y_j - c_j x) \tag{24b}$$

The initial value of the momentum conjugate to the hydrogen bond coordinate, p_x, and the initial values of the bath phase space variables, $\{\varpi_{y_O}, \varpi_{p_{y_O}}\}$, are sampled from the weight $e^{-\beta H_{eff}(x_{O=0}, p_{x_O}, \varpi_{y_O}, \varpi_{p_{y_O}})}$ via the Box-Muller algorithm[28]. The trajectories are performed with the leap-frog Verlet algorithm[29] and we find10,000 trajectories are enough to converge all results.

In Figs. 1 we see the classical rate constants vs. friction strength for the hydrogen transfer across a barrier of 15 kJ mol^{-1}. Figure 10 (a) is the fast friction time scale (800 f.s.) while Figure 10 (b) is the slow friction time scale (3000 f.s.). As can be seen, this

system shows the Kramer's turnover behavior. When the system has a large barrier height of 95 kJ mol^{-1} similar behavior is observed.

Fig. 11 (a) shows the classical and effective quantum potential at a slow time scale for a low barrier hydrogen bonded system. The effective quantum potential is graphed at two different values of friction strength. The short dashed line represents the effective quantum potential with a friction strength of 5.0 x 10^{-5}a.u., the long dashed line is the effective quantum potential with a friction strength of 1.0 x 10^{-5} a.u., and the classical potential is the solid line. This figure shows that the effective quantum potential approaches the classical potential as the friction strength increases. Thus, the quantum kinetic isotope effect should be diminishing in the high friction environment. This trend holds true as the barrier height increases and the low barrier hydrogen bonds turns into a high barrier hydrogen bond.

Fig. 11 (b) shows the classical and effective quantum potentials for a friction strength of 5.0 x 10^{-5} a.u. for a low barrier hydrogen bonded system. The effective quantum potential is graphed at two different values of the friction time scale. The short dashed line represents the effective quantum potential with a fast friction time scale, the long dashed line represents the effective quantum potential with a slow friction time scale, and the solid line represents the classical potential. This figure shows that the effective quantum potential approaches the classical potential in the fast friction time scale environment. Thus, the quantum kinetic isotope effect decreases as the solvent friction time scale increases.

Tables II-V show the rate constant ratios for deuteron to proton transfer across the 15 and 95 kJ mol^{-1} barrier heights at differing friction strengths and friction time scales.

Tables II and IV show that rate constant ratio is on the order of 10^{-1} in magnitude for the LBHB (15 kJ mol^{-1}) barrier height over a range of friction strengths and friction time scales. Tables III and V show that the rate constant is on the order of 10^{-4} to 10^{-6} in magnitude for the HBHB (95 kJ mol^{-1}) barrier height. Thus, there is a significant kinetic isotope effect that can be used to differentiate between weak and strong hydrogen bonded systems. The strong hydrogen bonded system has a rate constant ratio for deuteron to proton transfer on the order of 10^3 to 10^5 times greater than the rate constant ratio of the weak hydrogen bonded system at a given friction strength and time scale. The reason for this large isotope effect is the difference between the proton and deuteron's ability to tunnel through the barrier. The tunneling corrections becomes particularly important as the barrier height increases, and this large isotope effect is consistent (in order of magnitude) with a simple analytic expression that has been derived by others.[32]

One can detect two trends for the rate constant ratios in the weak hydrogen bonded system. First, as the friction strength increases in tables III and V the rate constant ratio increases. Thus, the kinetic isotope effect decreases as a function of increased friction strength. This can be explained by Fig. 11 (a) which shows the effective quantum potential approaching the Classical potential as the friction strength increases. The second trend that can be seen is that the rate constant ratios are smaller in the slow friction time scale regime (table V) as compared to the fast friction time scale regime (table III). This means that the kinetic isotope effect diminishes when the friction time scale quickens. This can be explained by Fig. 11 (b) which shows the effective quantum potential approaching the classical potential as the friction time scale quickens.

When one observes the, $\frac{\langle \chi_{eff} \rangle_D}{\langle \chi_{eff} \rangle_H}$ column in the tables (II – IV) it can be determined that the dynamical portion of Eq. (22) has a minor contribution on the rate constant ratio. Therefore Eq. (22) can be rewritten to only include the thermodynamic component. This estimation can be written as

$$\frac{\kappa_D}{\kappa_H} \approx \frac{e^{-\beta(D_{eff}^D - D_{eff}^H)}}{\varphi} \tag{25}$$

Tables VI and VII show the rate constant ratios using Eq. (25) over a range of barrier heights at moderate friction strengths for the two friction time scales, σ = 800 fs (table VI) and σ = 3000 fs (table VII). The tables show that for barrier heights 20 kJ mol^{-1} and less the rate constant ratio is $\leq 10^{-2}$, when greater than 20 kJ mol^{-1} this ratio is $> 10^{-2}$.

These results show that there is significant kinetic isotope effect on the transfer rate between donor and acceptor sites in a hydrogen bond. This effect, although easy to predict *a priori*, is quite complex in its details. If the hydrogen bond is weak (HBHB) then the isotope effect depends very strongly on the characteristics of the surrounding solvent. The Isotope effect depends very weakly on the surrounding solvent if the hydrogen bond is strong (LBHB). The isotope effect is at least two orders of magnitude larger (at a given friction strength and time scale) for the HBHB than for the LBHB. By contrast, the LBHB shows about the same value of the rate constant ratio $\frac{\kappa_D}{\kappa_H}$ for all friction strengths and time scales studied

CHAPTER 4

CONCLUSION

The goal of this work was to determine the possibility of detecting the presence of LBHB's with UV spectroscopy and present an approximate way to compute rate constants for proton transfer in a hydrogen bonded system in the presence of a solvent, and further, to quantify the expected kinetic isotope effects for proton transfer in a strongly hydrogen bonded system.

The UV spectra of hydrogen bonded systems was raised using the time-dependent view of spectroscopy. These simulations of this time-dependent view allowed us to interpret the spectral features in all different types of spectra. We find that the photodissociation, photoabsorption, and emission spectra of systems containing LBHB's have very distinctive features and can be an effective experimental method for detecting the presence of LBHB's.

In the photodissociation spectra there are two peaks in the UV spectra. As the strength of the LBHB increases the distance and resolution of the two peaks decrease.

The photoabsorption spectra for LBHB systems show a large absorption followed by a Franck-Condon vibronic progression. In systems that have a HBHB there is a large absorption followed by a Franck-Condon vibronic progression that is severly blue shifted.

The emission spectra for systems containing a LBHB have two distinct absorption peaks. As the LBHB loses it's strength the two peaks coalesce into a single emisson maximum.

Rate constants, for proton transfer in a hydrogen bonded system in the presence of a solvent, were determined by computing the classical reactive flux on an effective

quantum mechanical potential. It was found that the dynamical portion of the isotope effect is negligible, and the critical component of the kinetic isotope effect is the activation energy and the isotopic fractionation factor. We have found that for a LBHB system the ratio of deuteron to hydrogen transfer is on the order of 10^{-1} for barriers below 15 kJ/mol, regardless of the friction strength and friction time scale. Alternatively, for weak , high barrier hydrogen bonds, this deuteron to hydrogen transfer ratio is on the order of 10^{-6} in the weak friction regime and 10^{-4} in the stronger friction regime. This demonstrates quite a difference in the rate constant ratios and thus creates an extremely large isotope effect. This large isotope effect is due to the large difference between the ability of the proton and deuteron to tunnel through the barrier.

Table I

A (a.u.)	B (a.u.)	Barrier (kJ/mol)
0.1	0.1	65.63
0.1	0.05	16.41
0.1	0.035	8.04

Table II Barrier Height = 15 kJ/mol and σ = 800 fs.

friction strength	φ	$e^{-\beta(D_{eff}^{D}-D_{eff}^{H})}$	$\left(\frac{\langle\chi_{eff}\rangle_{D}}{\langle\chi_{eff}\rangle_{H}}\right)$	$\left(\frac{\kappa_{D}}{\kappa_{H}}\right)$
2.00×10^{-5}	2.5	0.17	1.0	0.07
3.00×10^{-5}	2.5	0.21	1.3	0.11
4.00×10^{-5}	2.4	0.29	0.6	0.08
5.00×10^{-5}	2.4	0.33	0.8	0.11

Table III Barrier Height = 95 kJ/mol and σ = 800 fs.

friction strength	φ	$e^{-\beta(D_{eff}^{D}-D_{eff}^{H})}$	$\left(\frac{\langle\chi_{eff}\rangle_{D}}{\langle\chi_{eff}\rangle_{H}}\right)$	$\left(\frac{\kappa_{D}}{\kappa_{H}}\right)$
2.00×10^{-5}	7.5	1.2×10^{-5}	0.9	1.5×10^{-6}
3.00×10^{-5}	7.0	6.7×10^{-5}	0.7	6.2×10^{-6}
4.00×10^{-5}	6.7	5.6×10^{-3}	0.5	3.8×10^{-4}
5.00×10^{-5}	6.4	1.1×10^{-2}	0.5	8.3×10^{-4}

Table IV Barrier Height = 15 kJ/mol and σ = 3000 fs.

friction strength	φ	$e^{-\beta(D_{eff}^{D}-D_{eff}^{H})}$	$\left(\frac{\langle \chi_{eff} \rangle_{D}}{\langle \chi_{eff} \rangle_{H}}\right)$	$\left(\frac{\kappa_{D}}{\kappa_{H}}\right)$
3.0×10^{-5}	2.6	0.18	1.5	0.10
5.0×10^{-5}	2.6	0.17	1.1	0.07
8.0×10^{-5}	2.5	0.18	1.1	0.08
1.0×10^{-4}	2.5	0.27	1.1	0.12

Table V Barrier Height = 95 kJ/mol and σ = 3000 fs.

friction strength	φ	$e^{-\beta(D_{eff}^{D}-D_{eff}^{H})}$	$\left(\frac{\langle \chi_{eff} \rangle_{D}}{\langle \chi_{eff} \rangle_{H}}\right)$	$\left(\frac{\kappa_{D}}{\kappa_{H}}\right)$
3.0×10^{-5}	8.1	7.1×10^{-6}	2.2	1.9×10^{-6}
5.0×10^{-5}	7.8	9.5×10^{-6}	1.9	2.4×10^{-6}
8.0×10^{-5}	7.3	2.9×10^{-5}	1.2	4.8×10^{-6}
1.0×10^{-4}	7.1	1.8×10^{-4}	0.7	1.7×10^{-5}

Table VI Friction strength = 5 x 10^{-5} and σ = 800 fs.

Barrier Height (kJ/mol)	φ	$e^{-\beta(D_{eff}^{D}-D_{eff}^{H})}$	$\left(\frac{\kappa_D}{\kappa_H}\right)$
10	2.0	0.30	0.15
20	2.9	0.14	4.6 x 10^{-2}
40	4.4	0.02	4.1 x 10^{-3}
60	5.6	7.8 x 10^{-4}	1.4 x 10^{-4}
80	7.2	1.0 x 10^{-5}	1.5 x 10^{-6}

Table VII Friction Strength = 3 x 10^{-5} and σ = 3000 fs.

Barrier Height (kJ/mol)	φ	$e^{-\beta(D_{eff}^{D}-D_{eff}^{H})}$	$\left(\frac{\kappa_D}{\kappa_H}\right)$
10	1.9	0.24	0.13
20	3.0	0.08	2.7 x 10^{-2}
40	4.8	7.7 x 10^{-3}	1.6 x 10^{-3}
60	6.1	2.4 x 10^{-4}	4.0 x 10^{-5}
80	7.8	5.1 x 10^{-6}	6.6 x 10^{-7}

Butler, et. al., "On the possibility of using UV...", Fig 1 (a)

Butler, et. al., "On the possibility of using UV...", Fig 1 (b)

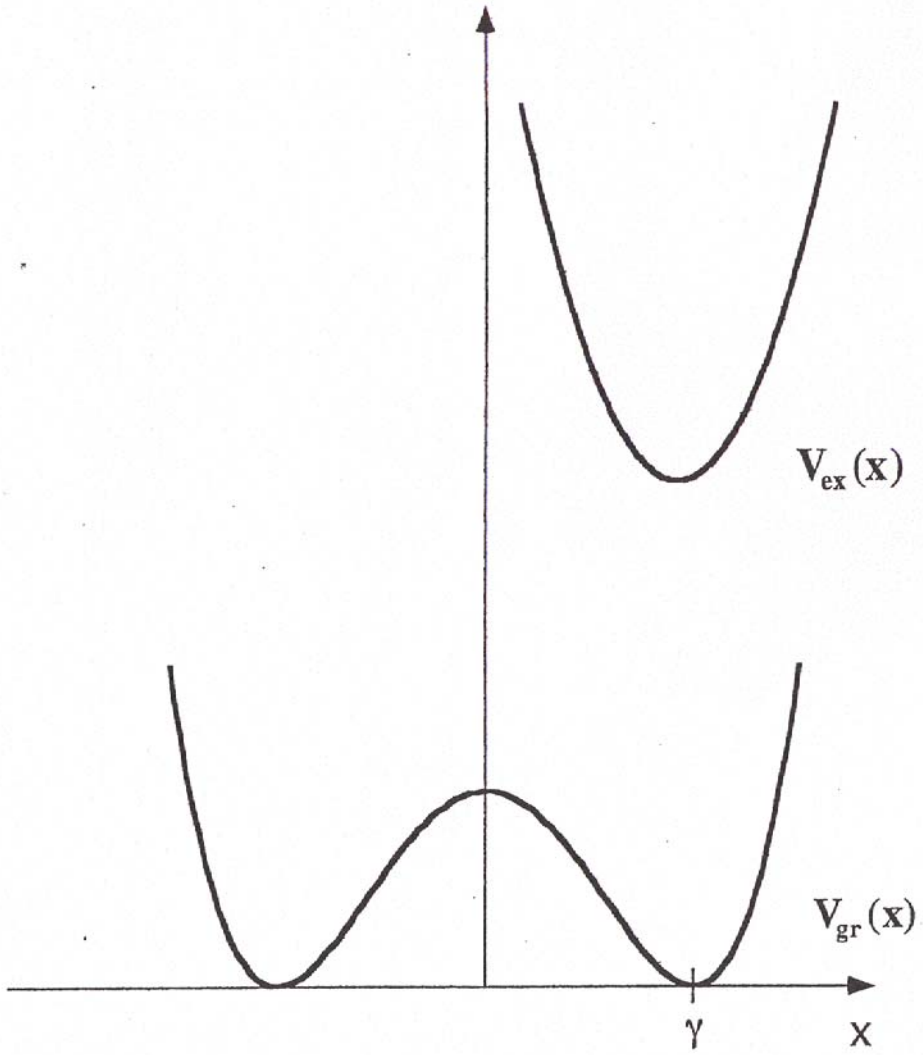

Butler, et. al., "On the possibility of using UV...", Fig 2 (a)
ψ(x)
-1
-0.5
0
0.5
1
x(Å)

Butler, et. al., "On the possibility of using UV...", Fig 2 (b)

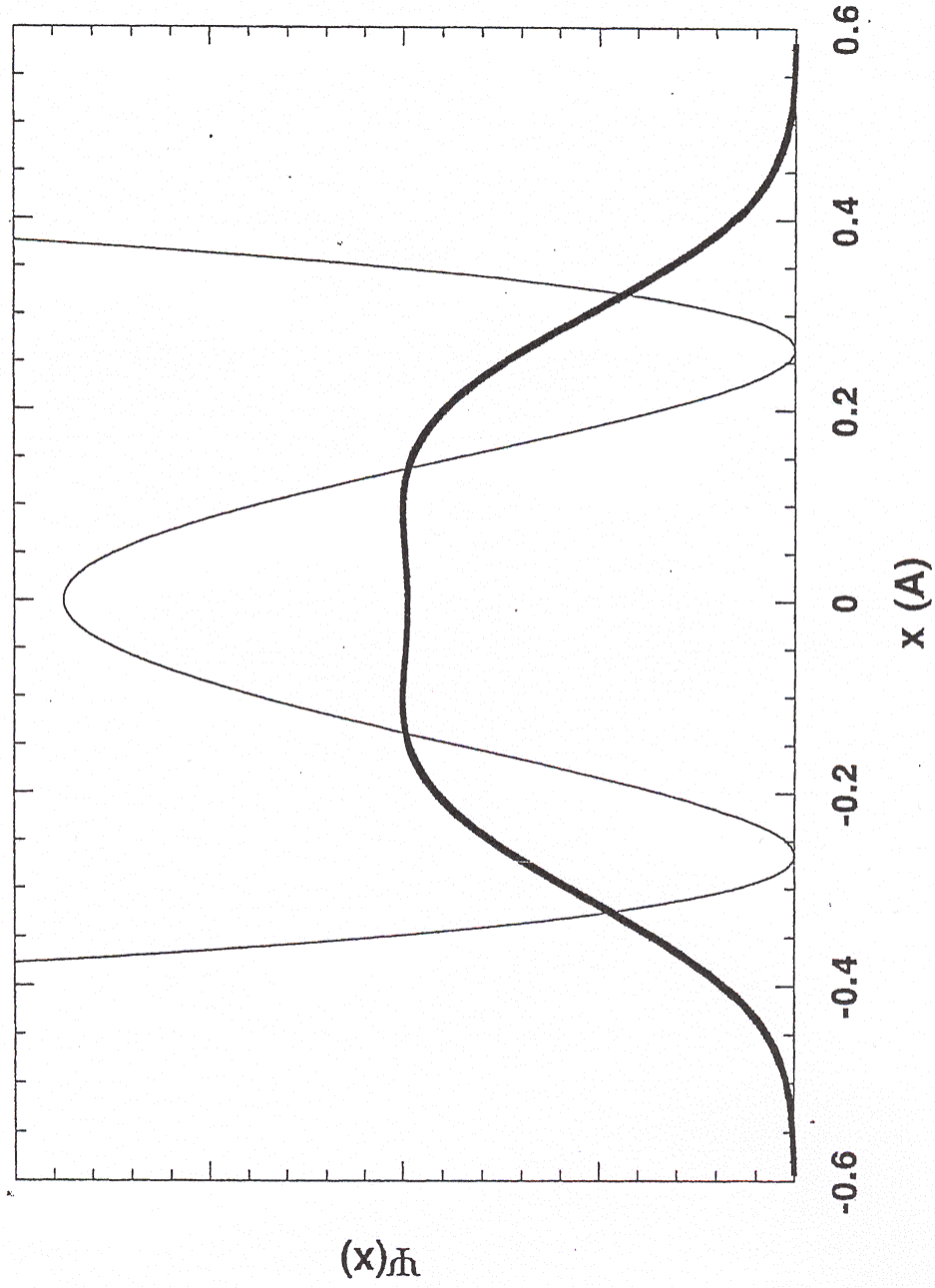

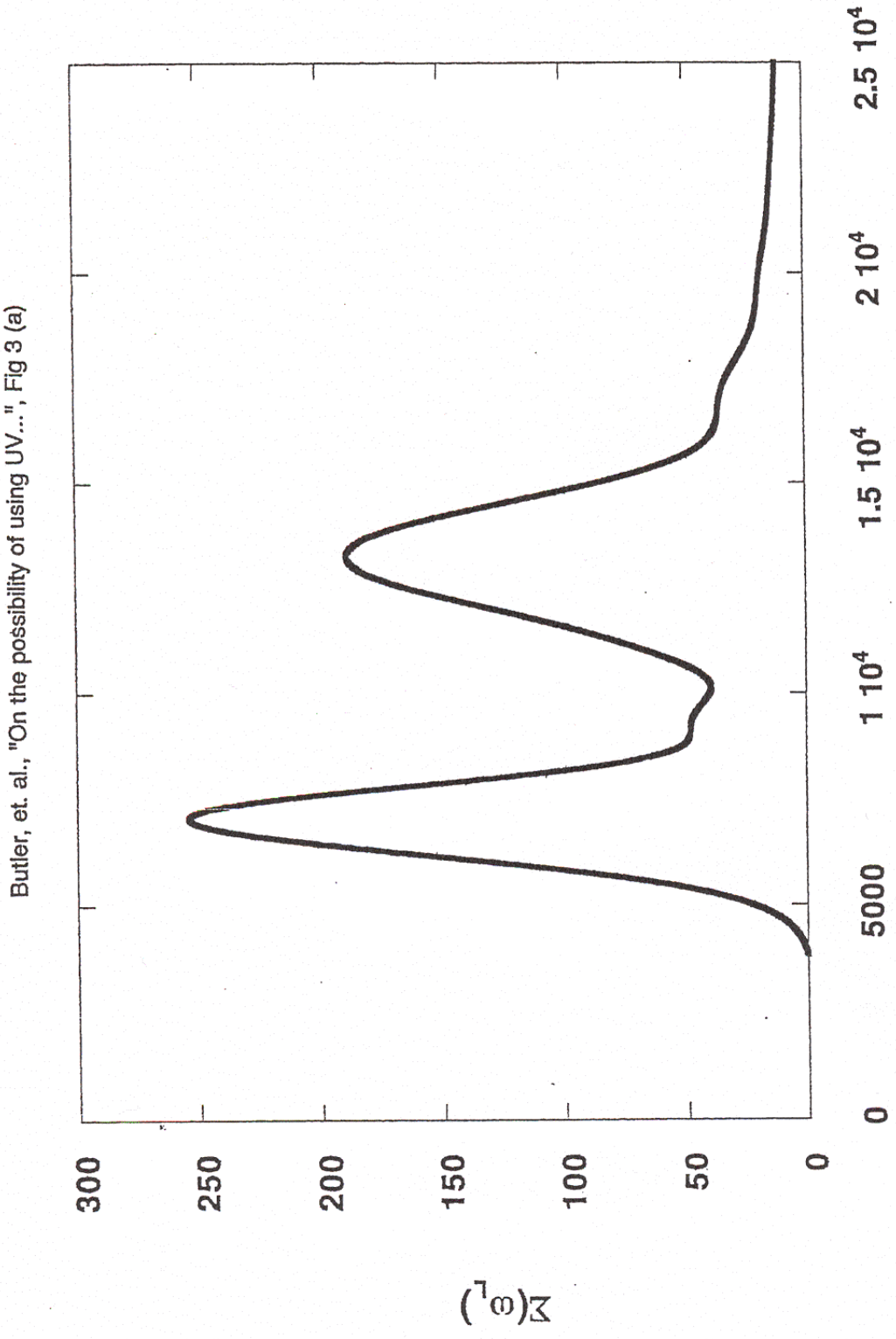
Butler, et. al., "On the possibility of using UV...", Fig 3 (a)
Σ(ω_L)
300
250
200
150
100
50
0
0
5000
1 10^4
1.5 10^4
2 10^4
2.5 10^4
ω(cm^-1)

Butler, et. al., "On the possibility of using UV...", Fig 3 (b)

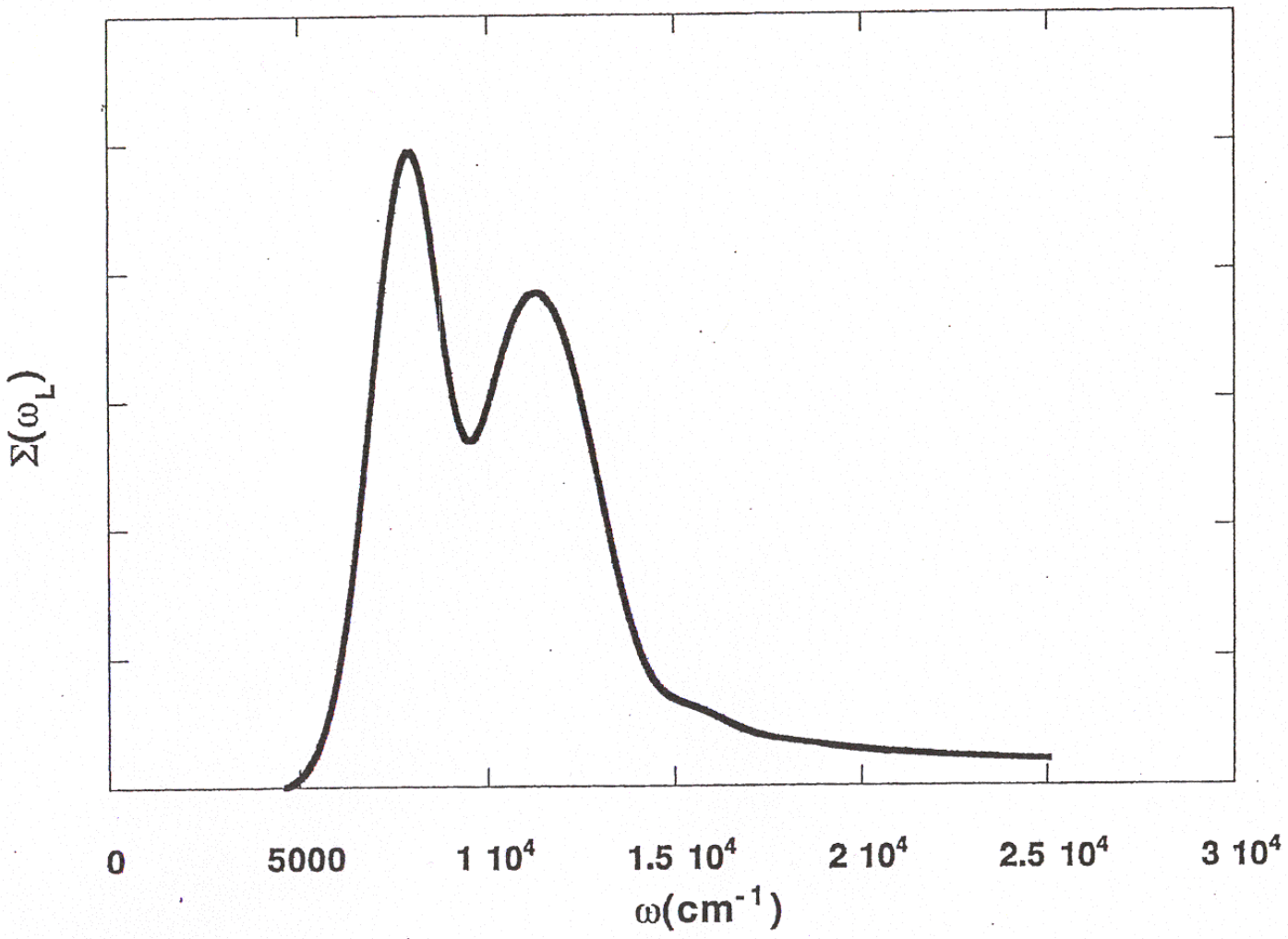

Butler, et. al., "On the possibility of using UV...", Fig 3 (c)

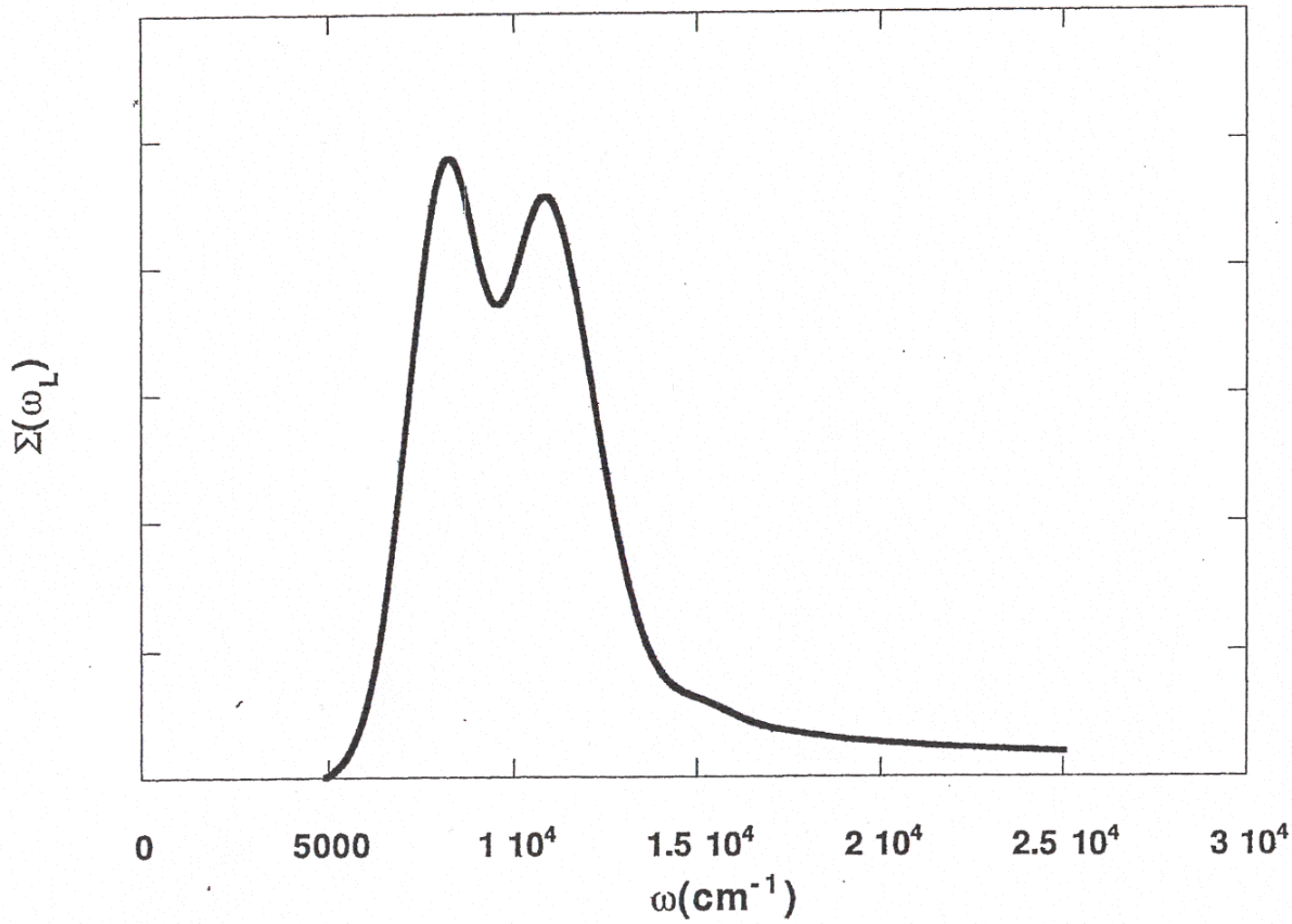

Butler, et. al., "On the possibility of using UV...", Fig 4

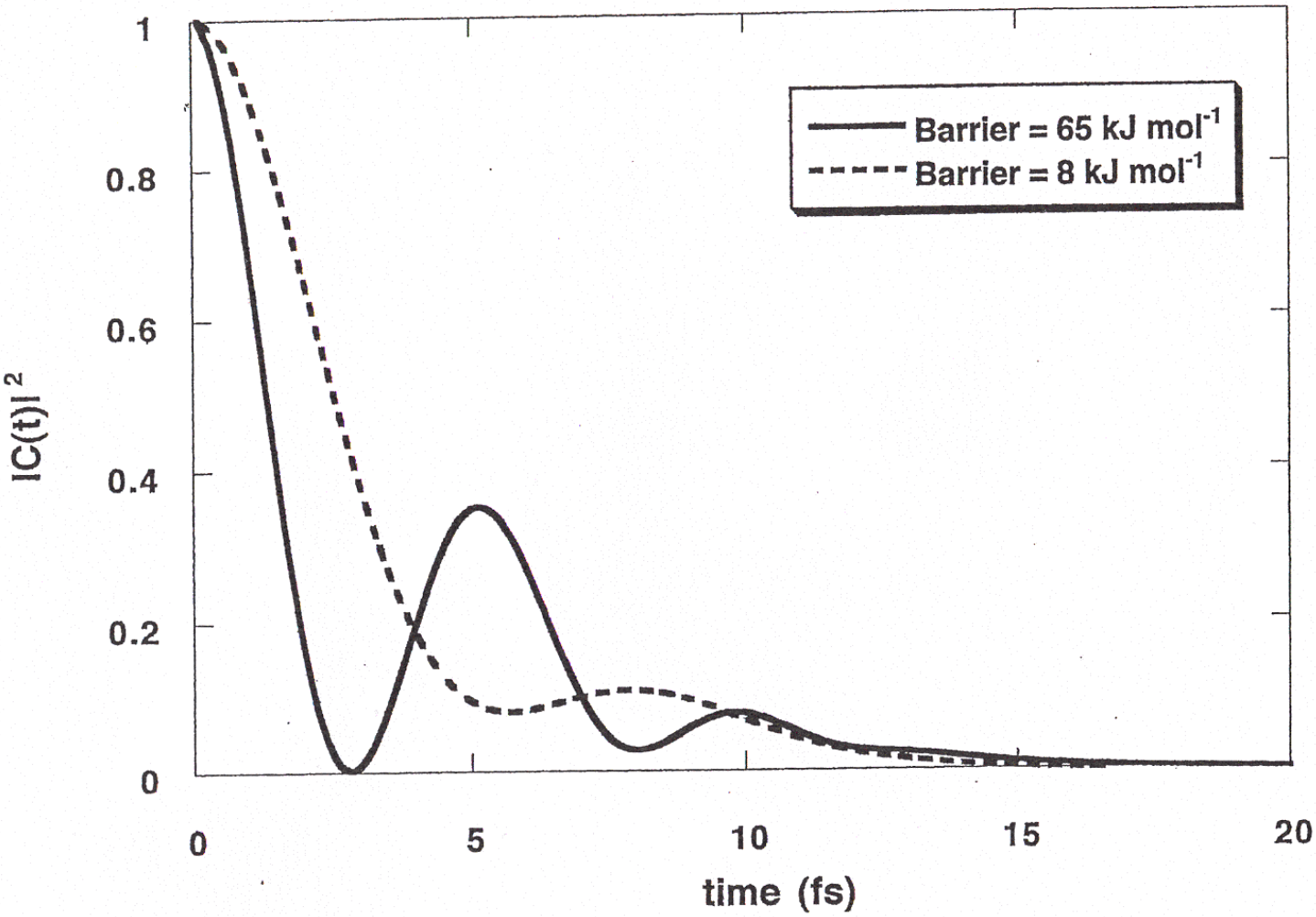

Butler, et. al., "On the possibility of using UV...", Fig. 5

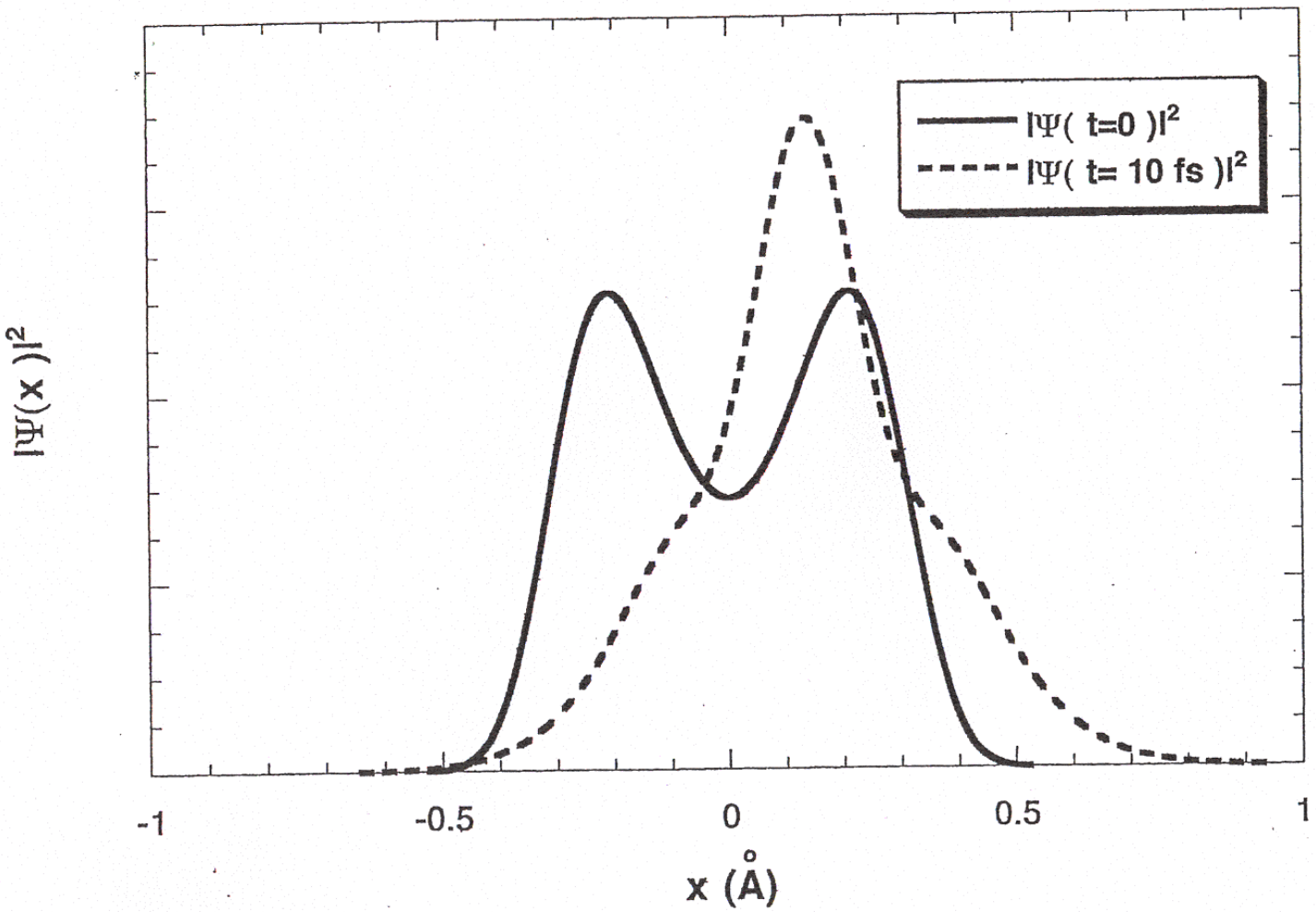

Butler, et. al., "On the possibility of using UV..."; Fig 6

Butler, et. al., "On the possibility of using UV...", Fig 7 (a)

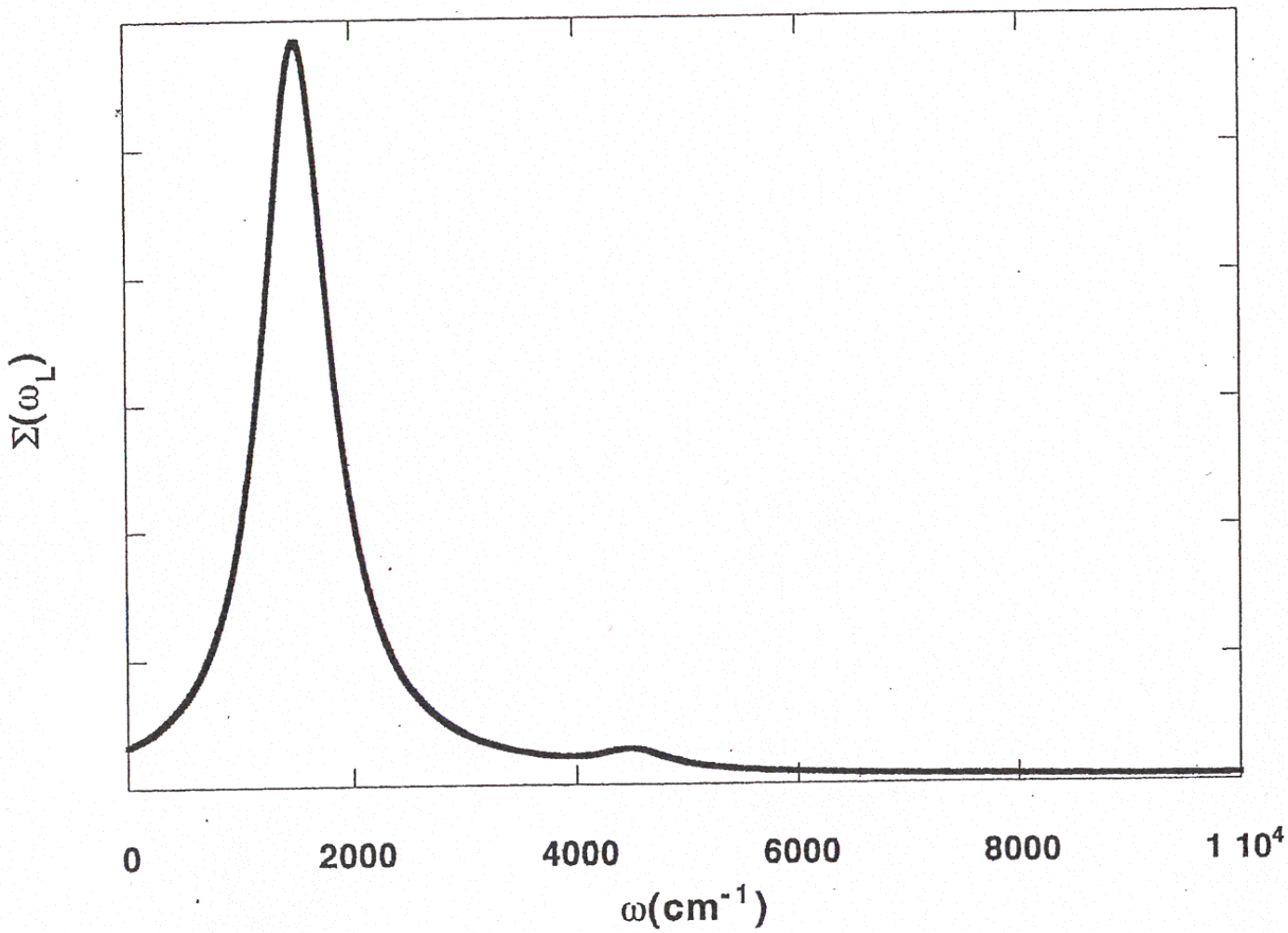

Butler, et. al., "On the possibility of using UV...", Fig 7 (b)

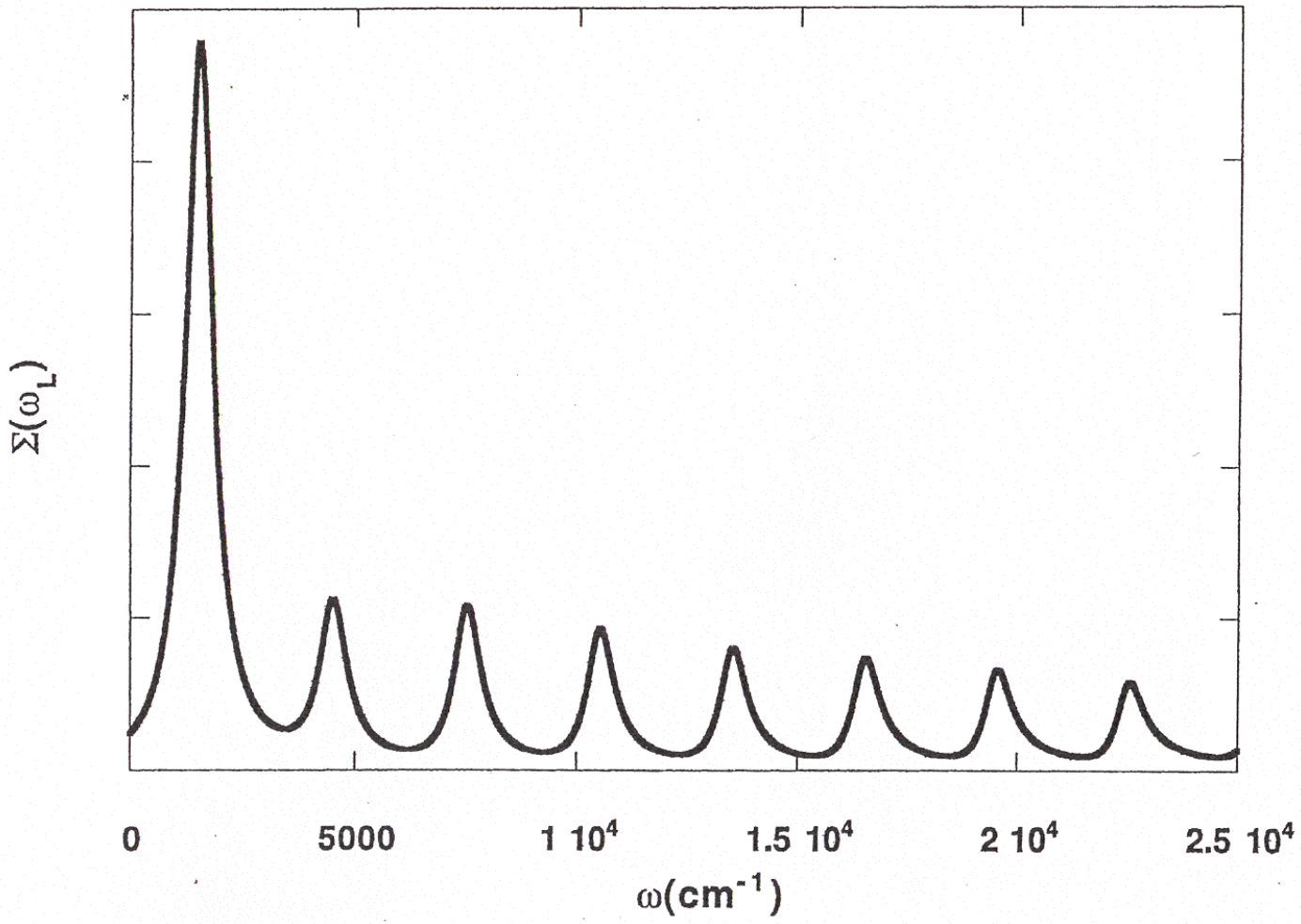

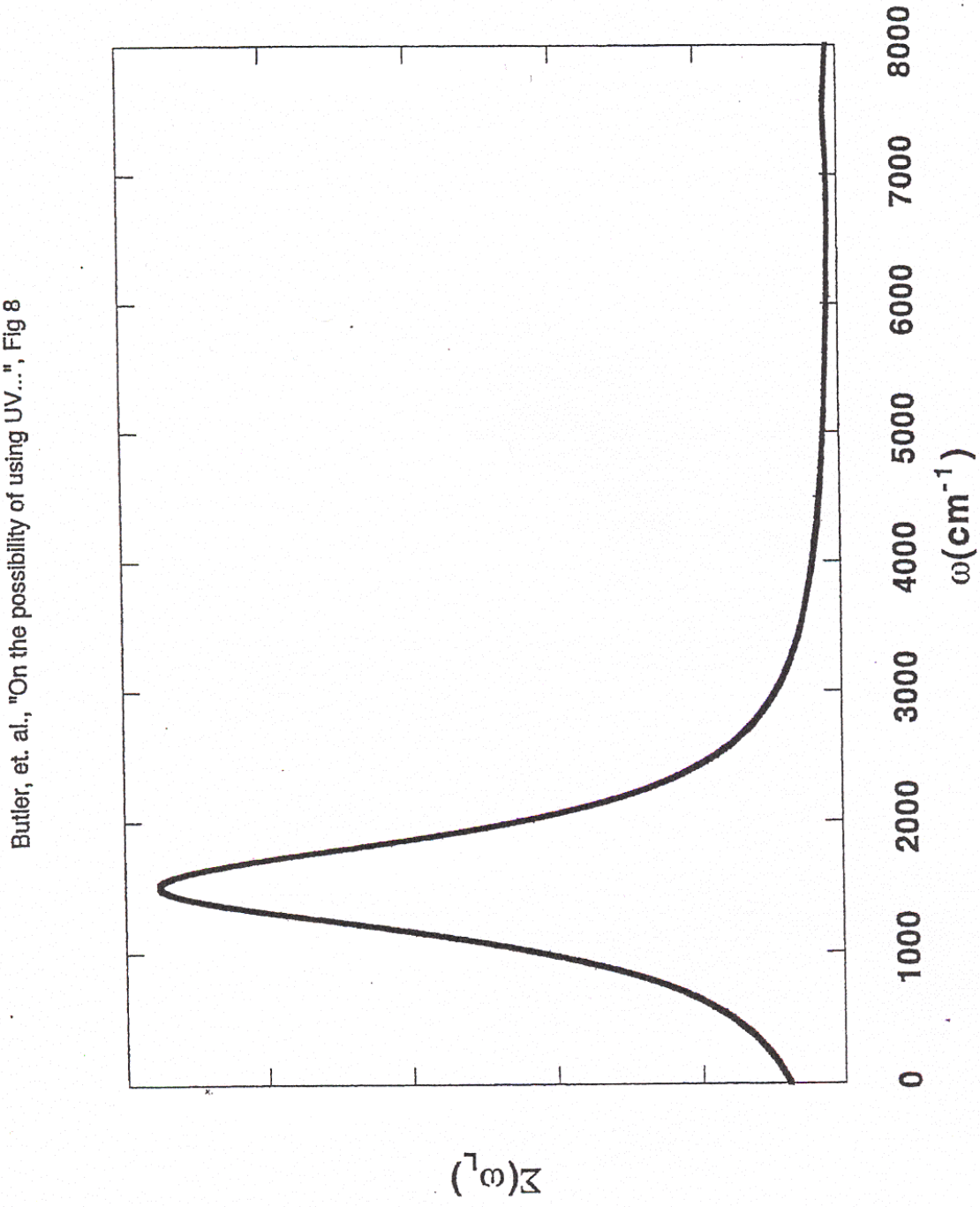
Butler, et. al., "On the possibility of using UV...", Fig 8
Σ(ω_L)
0
1000
2000
3000
4000
5000
6000
7000
8000
ω(cm^-1)

Butler, et. al., "On the possibility of using UV...", Fig 9 (a)

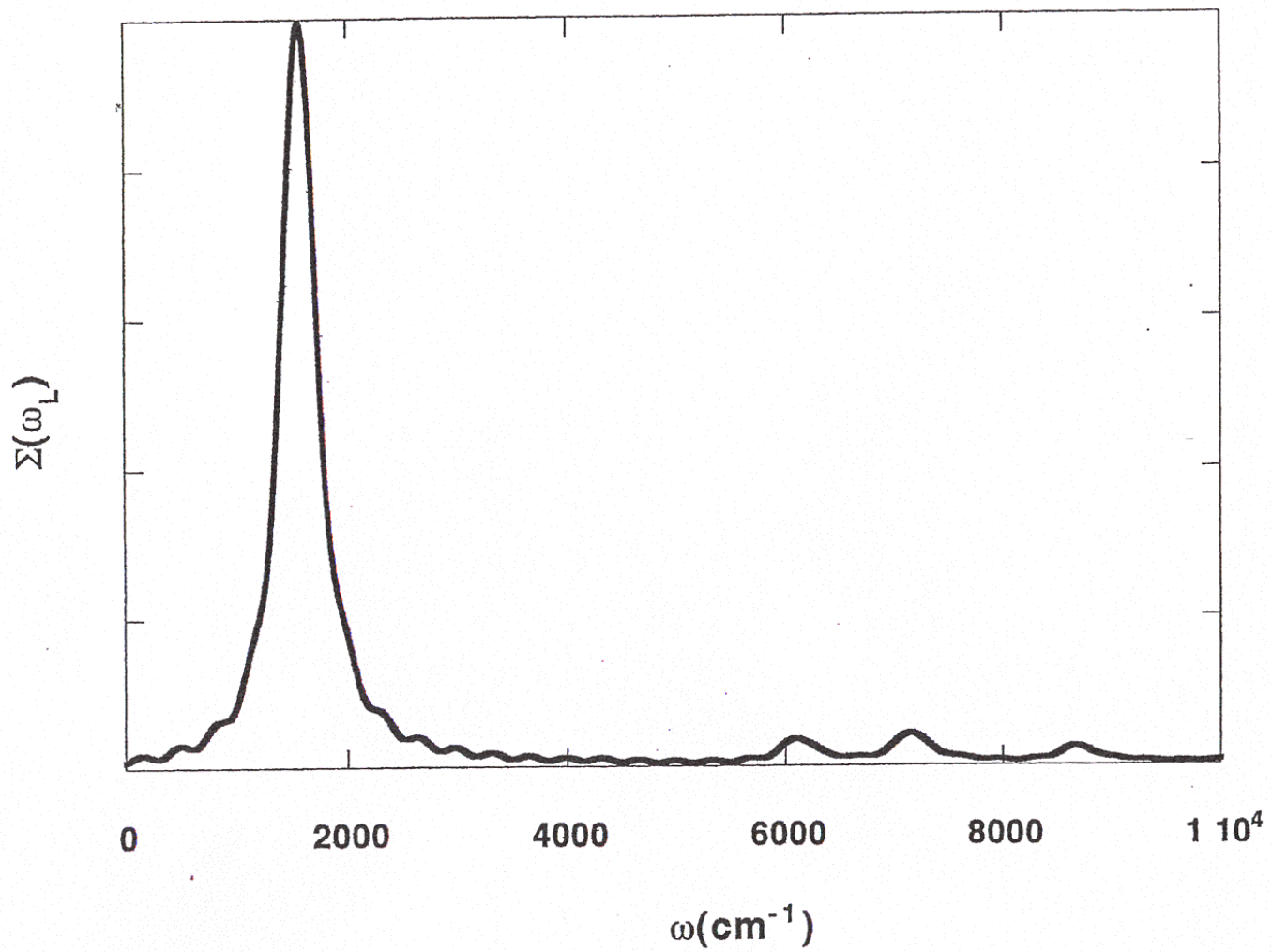

Butler, et. al., "On the possibility of using UV...", Fig 9 (b)

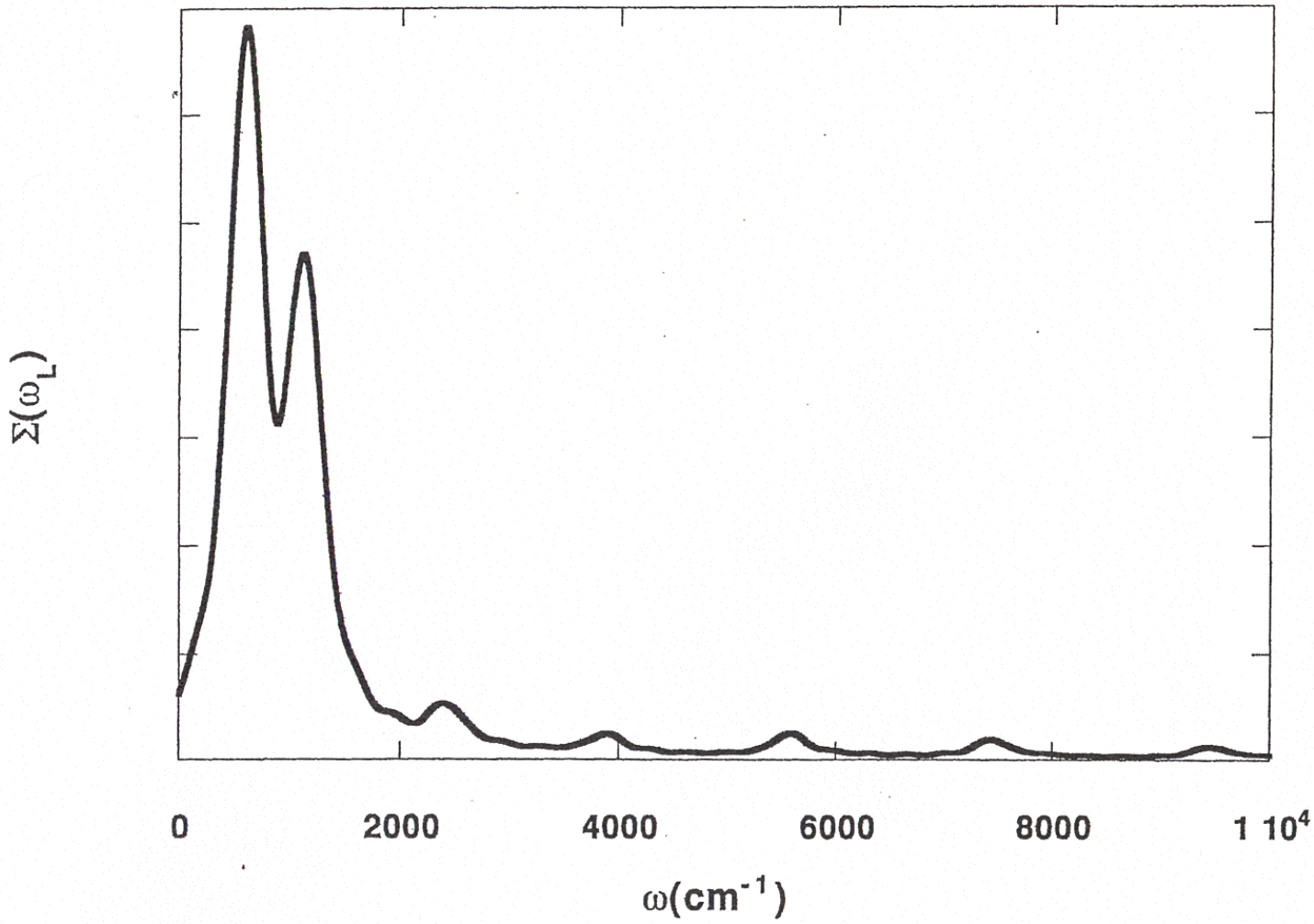

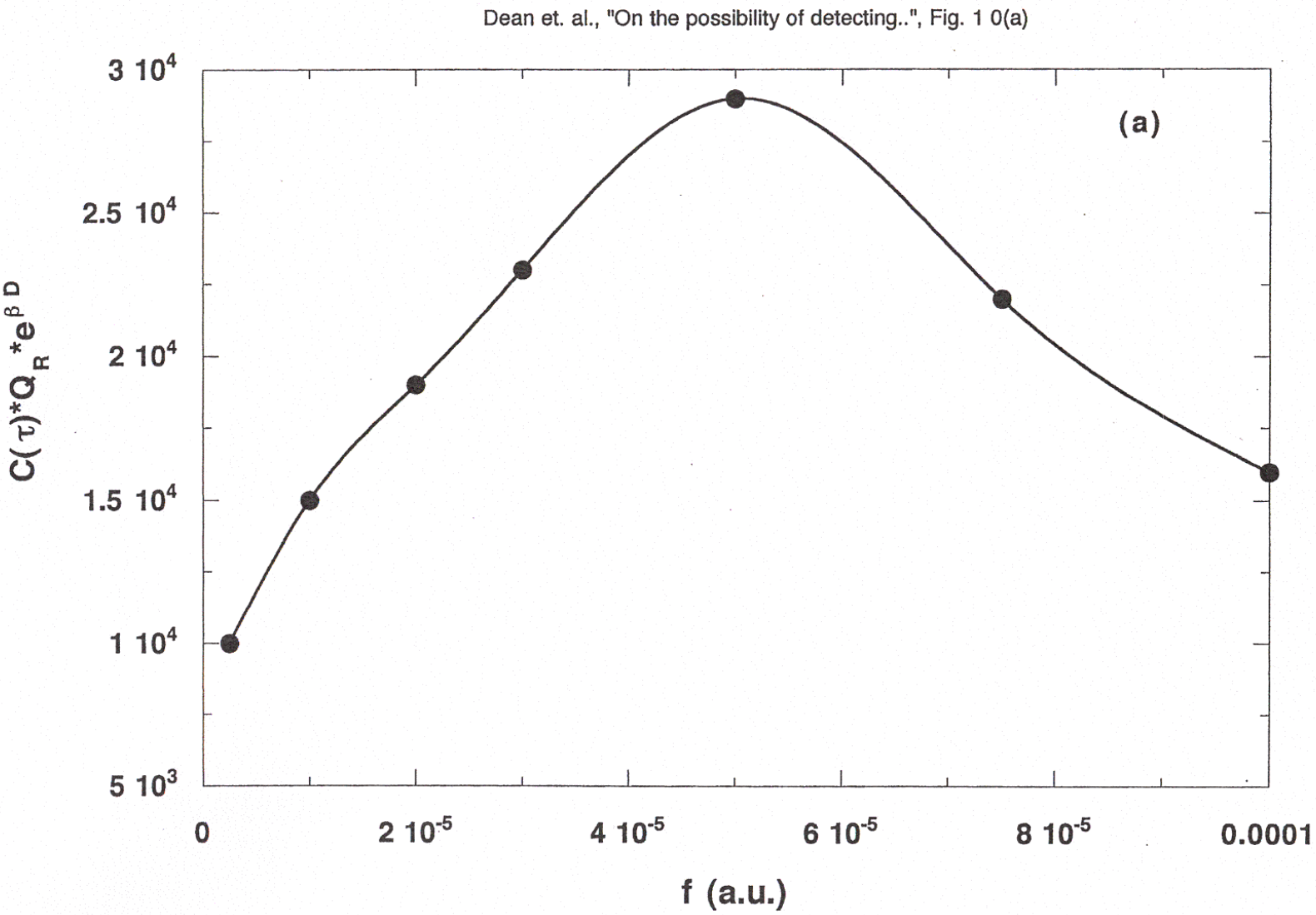
Dean et. al., "On the possibility of detecting..", Fig. 1 0(a)
(a)
3 10^4
2.5 10^4
2 10^4
1.5 10^4
1 10^4
5 10^3
C(τ)*Q_R*e^βD
0
2 10^-5
4 10^-5
6 10^-5
8 10^-5
0.0001
f (a.u.)

Dean et. al., "On the possibility of detecting..", Fig. 10 (b)

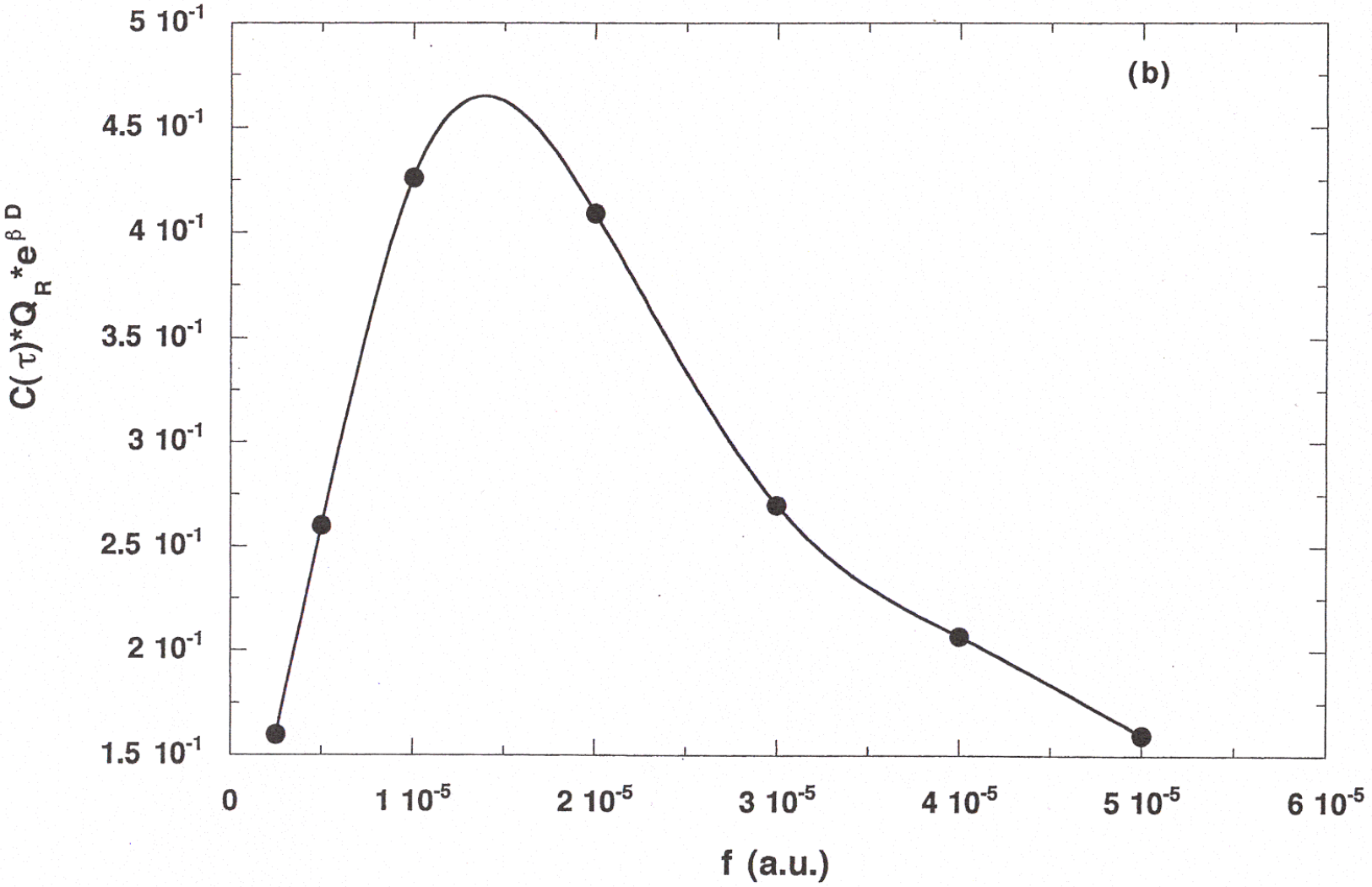

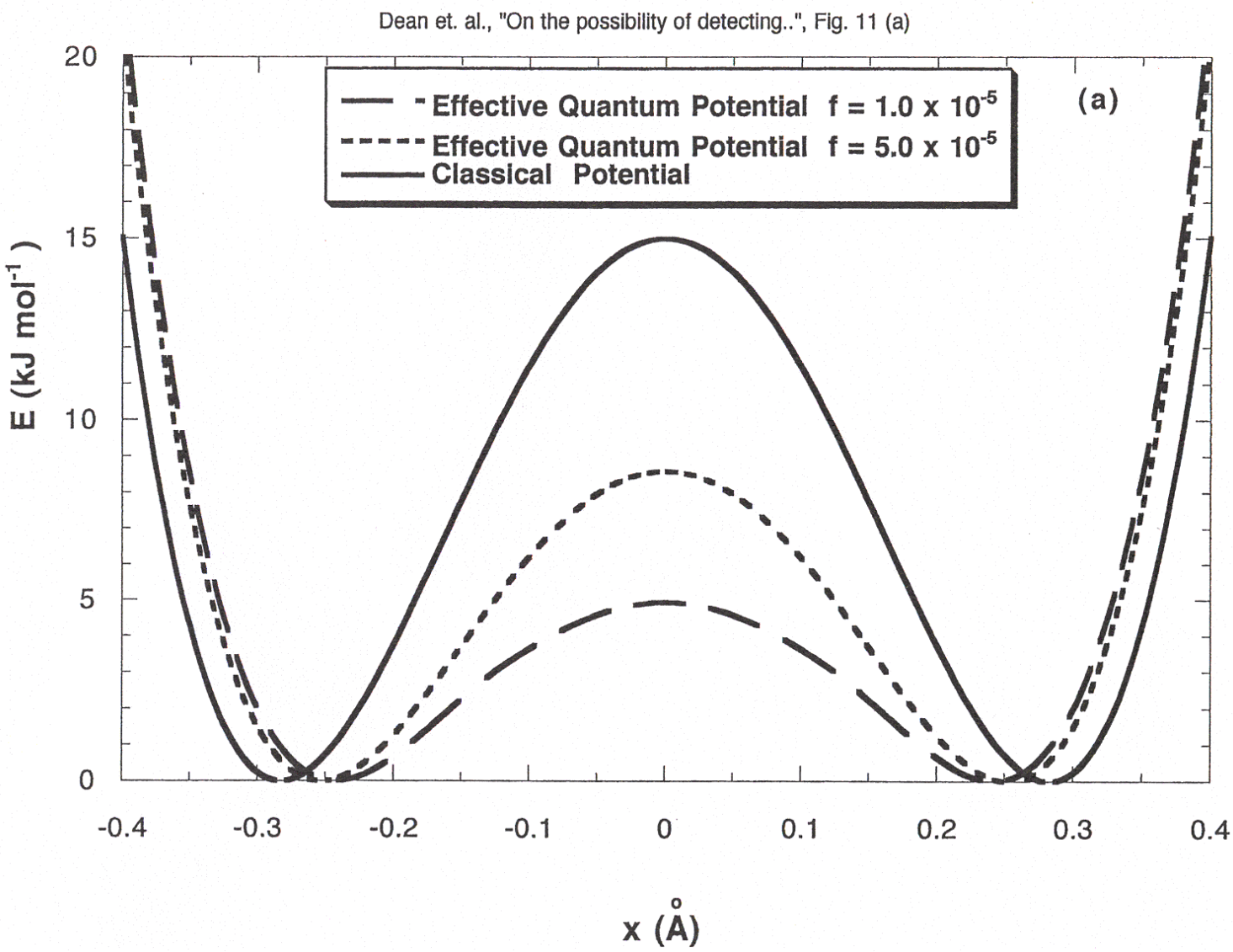
Dean et. al., "On the possibility of detecting..", Fig. 11 (a)
Effective Quantum Potential f = 1.0 x 10-5
Effective Quantum Potential f = 5.0 x 10-5
Classical Potential
(a)
E (kJ mol-1)
x (Å)
20
15
10
5
0
-0.4
-0.3
-0.2
-0.1
0
0.1
0.2
0.3
0.4

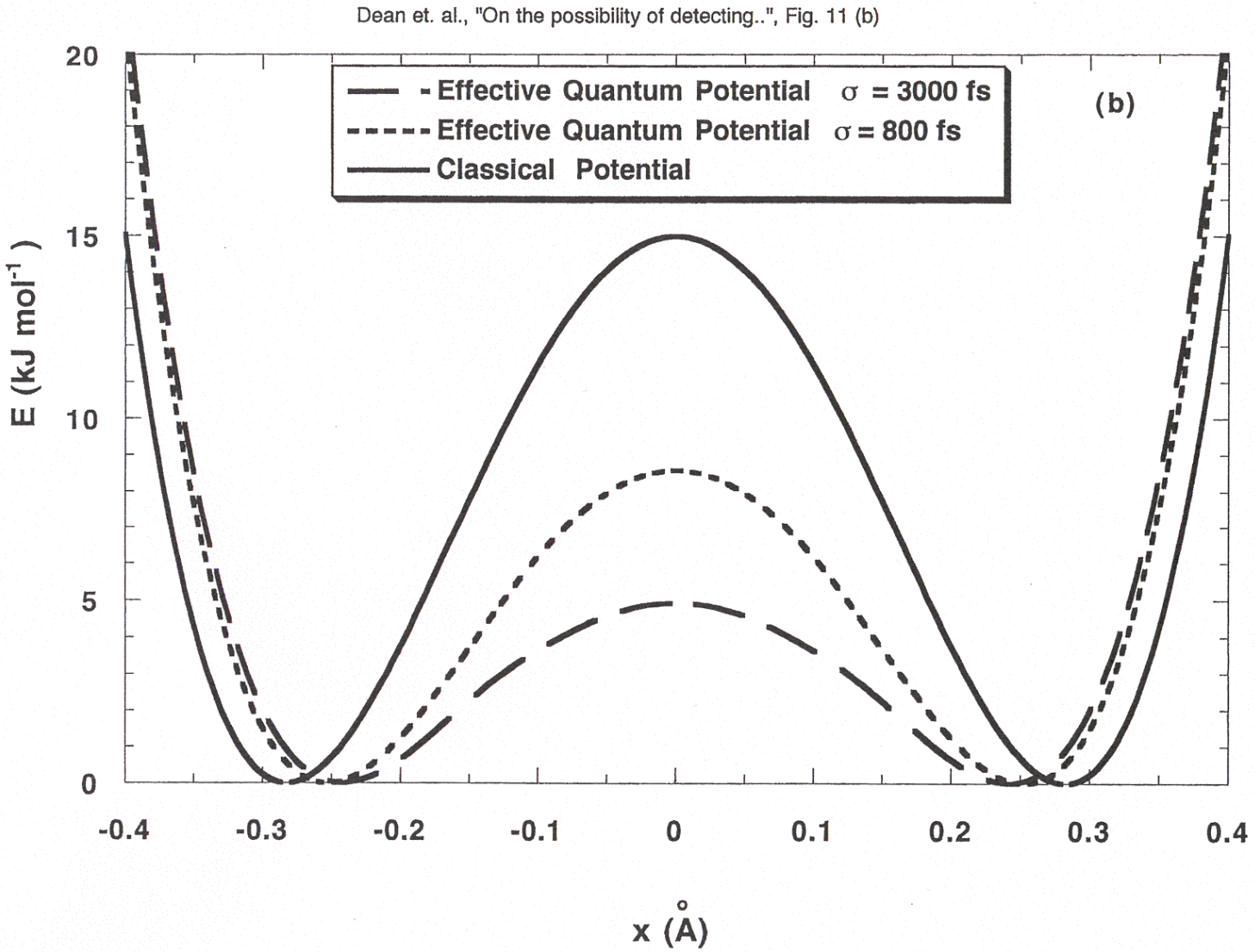
Dean et. al., "On the possibility of detecting..", Fig. 11 (b)
Effective Quantum Potential σ = 3000 fs
Effective Quantum Potential σ = 800 fs
Classical Potential
(b)
E (kJ mol-1)
20
15
10
5
0
-0.4
-0.3
-0.2
-0.1
0
0.1
0.2
0.3
0.4
x (Å)

REFERENCES

1. Cleland, W. W.; Kreevoy, M. M. *Science* 1994, 264, 1887.
2. Guthrie, J.P. *Chem. Biol.* 1996, 3, 163.
3. Frey, P. A.; Whitt, S. A.; Tobin, J. B. *Science* 1994, 264, 1927.
4. Neidhart, D.; Wie, Y.; Cassidy, C.; Lin, J.; Cleland, W. W.; Frey, P. A. *Biochemistry* , 40, 2439.
5. Shan, S.; Herschlag, D. *Proc. Natl. Acad. Sci.* USA 1996, 93, 14474.
6. Cassidy, C.; Lin, J.; Frey, P. A. *Biochemistry* 1997, 36, 4576.
7. Kreevoy, M. M.; Liang, T. M. *J. Am. Chem. Soc.* 1980, 102, 3315.
8. Lin, J.; Westler, W.M.; Cleland, W.W.; Markley, J.L.; Frey, P.A. *Biochemistry* 1995, 34, 4516.
9. Speakman, J.C. *J. Chem. Soc.* 1949, 3357.
10. Altman, L. J.; Laungani, D.; Gannarsson, G.; Wennerstrom, H.; Forsen, S. *J. Am. Chem. Soc.* 1978, 100, 8264.
11. Madsen, G.; Iversen, B.; Larsen, F.; Kapon, M.; Reisner, G.; Herbstein, F. *J. Am. Chem. Soc.* 1998, 120, 10040.
12. Harris, T.K.; Mildvan, A.S. Proteins: Structure, Function, and Genetics 1999, 35, 275.
13. Pimentel, G.C.; McClellan, A.L. *The Hydrogen Bond.* 1960, 85.
14. Heller, E.J.; *Accts. Chem. Res.* 1981, 14, 368.
15. Hadzi, D. *Pure Appl. Chem*. 1965, 11, 435.
16. Heller, E. J. *Accts. Chem. Res*. 1981, 14, 368.
17. Baym, G. *Lectures on Quantum Mechanics*, University of Illinois: Canada, 1990.

18. Gordon, R. G. *Adv. Mag. Resonance*. 1968, 3, 1.

19. Ventura, K. M.; Greene, S. N.; Halkides, C.J.; Messina, M. *Structural Chemistry* 2001, 12, 23.

20. Feit, M.D.; Fleck Jr., J. A.; Steiger, A. *J. Computat. Phys*. 1982, 47, 412.

21. Herzberg, G. *Molecular Spectra and Molecular Structure* : New York, 1950.

22. Schenter, G.K.; Messina, M.; Garret, B.C. *J. Chem. Phys.* 1993, 99, 1674.

23. Hanggi, P.; Talkner, P.; Borkovec, M. *Reviews of Modern Physics.* 1990, 62, 251.

24. Chandler, D.; *J. Chem. Phys.* 1978, 68, 2959.

25. McRae, R.P.; Schenter, G.K.; Garrett, B.C.; Haynes, G.R.; Voth, G.A., and Schatz, G.C. *J. Chem. Phys.* 1992, 97, 7392.

26. Messina, M.; Schenter, G.K.; Garret, B.C. *J. Chem. Phys.* 98, 4120.

27. Skodje, R.T.; Truhlar, D.G. *J. Chem. Phys*. 1981, 85, 624.

28. Press, W.H.; Teukolsky, S.A.; Vetterling, W.T.; Flannery, B.P. *Numerical recipes in Fortran 77* 1992, Cambridge University, New York.

29. Allen, M.P.; Tildesley, D.J. *Computer Simulations of liquids*, 1987, Oxford.

30. Sagnella, D.E.; Cao, J.; Voth, G.A. *J. Chem. Phys.* 1994, 180, 167-180.

31. (a) Cao, J.; Voth, G.A. *J. Chem. Phys*. 1994, 100, 5106-5117 ; (b) Cao, J.; Voth G.A. *J. Chem. Phys.* 1994, 101, 6157-6167 ; (c) Cao, J.; Voth, G.A. *J. Chem. Phys.* 1994, 101, 6168-6183.

32. Hanggi, P.; Grabert, H.; Ingold, G.L.; Weiss, U. *Phys. Rev. Lett.* 1985, 55, 761.